NOLTR 67-156

AN ANALYSIS OF THE SPLIT HOPKINSON PRESSURE BAR

2 OCTOBER 1967

NOL

UNITED STATES NAVAL ORDNANCE LABORATORY, WHITE OAK, MARYLAND

NOLTR 67-156

81

UNCLASSIFIED
NOLTR 67-156

AN ANALYSIS OF THE SPLIT HOPKINSON PRESSURE BAR

Prepared by:
James L. Rand

ABSTRACT: The purpose of this paper is to analyze in detail many of the assumptions and techniques often employed to obtain stress-strain relations at rates of strain of approximately 10^3 sec^{-1}. The effects of axial wave propagation and interaction detail in short cylindrical specimens on the resulting stress-strain relation have been evaluated in detail. The effect of specimen geometry on the "end effects" associated with friction has been clearly demonstrated both theoretically and experimentally. An overall evaluation of the quality of the data generated by the split Hopkinson pressure bar experiment based on a one-dimensional wave analysis and verified by experimental observations has been presented.

U. S. NAVAL ORDNANCE LABORATORY
WHITE OAK, SILVER SPRING, MARYLAND

NOLTR 67-156 2 October 1967

AN ANALYSIS OF THE SPLIT HOPKINSON PRESSURE BAR

This publication is part of the continuing effort of the U. S. Naval Ordnance Laboratory in the determination of dynamic properties of materials. The contents of this report are based in part on a dissertation by the author submitted to the Faculty of the Graduate School of the University of Maryland in partial fulfillment of the requirements for the degree of Doctor of Philosophy.

The author wishes to thank Professor John W. Jackson for his many suggestions. In addition, the cooperation and suggestions of those individuals and organizations interested in the determination of dynamic properties of materials is gratefully acknowledged.

E. F. SCHREITER
Captain, USN
Commander

a.e. Seigel

A. E. SEIGEL
By direction

CONTENTS

ILLUSTRATIONS

TABLES

LIST OF SYMBOLS

a	- Lagrangian coordinate; radius of specimen
A	- cross-sectional area; arbitrary constant
$\overline{A}$	- non-dimensional area, A_s/A
B	- constant defined by equation (A-31)
c	- wave speed, propagation velocity
$\overline{C}$	- non-dimensional wave speed defined by $c(\rho_s/E_s)^{\frac{1}{2}}$
d	- diameter
E	- elastic modulus
$\overline{E}$	- non-dimensional strain defined by ϵ/ϵ_y
F	- force
G	- gage factor (2.09 $\pm$.5%)
I	- impedance defined by equation (2)
K	- constant - defined as used
ℓ	- length
m	- mass
n	- constant defined by equation (C-2)
P	- non-dimensional impact function defined by $\int(\overline{C}_s)^{-1} dS$
r	- radial distance
R	- I_p/I_s; electrical resistance
S	- non-dimensional stress defined as σ/σ_y
t	- time
T, $\overline{T}$	- non-dimensional time defined as $c_o t/\ell_o$
U	- non-dimensional velocity defined as $(E_s\rho_s)^{\frac{1}{2}}v/\sigma_y$
v	- particle velocity
V	- voltage

x	- longitudinal coordinate
α	- parameter defined by equation (8).
β	- parameter defined as $\mu(d_o/\ell_o)$
ε	- "engineering" strain
θ	- energy defined by equation (15)
μ	- coefficient of friction
ρ	- mass density
$\bar{\rho}$	- non-dimensional density defined as ρ_s/ρ
σ	- "engineering" stress
τ	- time
φ	- impact function defined by equation (A-21)

SUBSCRIPTS

a	- "apparent" value
cal	- calibrated value
D	- refers to "dynamic" value
G	- refers to "gage"
I	- refers to incident pressure bar
L	- index on length in CASH code
LMAX	- maximum index on length in CASH code
m	- measured quantity
max	- maximum value
N	- index on time in CASH code
o	- elastic value; original value; or yield value as used
p	- refers to pressure bars
r	- refers to radial direction
R	- refers to reflected strain
s	- refers to specimen

T - refers to transmitter pressure bar

y - refers to the yield point of the specimen

z - refers to axial direction

θ - refers to tangential direction

SUPERSCRIPTS

$\dot{}$ - denotes differentiation with respect to time

INTRODUCTION

The behavior of materials under dynamic loading is receiving an increasing amount of attention as more highly transient environments are encountered. In order to simulate the rates of loading produced by impact or blast wave impingement, strain rates from 50 sec^{-1} to 10^4 sec^{-1} must be achieved. Various types of impact testing devices have been used [1]* which not only permit but require the existence of inertial forces or stress waves in the specimen in order to determine its stress-strain-strain rate relationship. One of the more popular devices of this type is the split Hopkinson pressure bar. This technique consists of placing a short specimen between a pair of bars which remain elastic while a stress wave is propagated through the system. When one-dimensional wave analysis is applied to the measured strain records from each bar, both the force and velocity at the specimen end of each bar can be calculated. The stress and strain of the specimen at any instant of time is obtained by averaging the forces and velocities obtained from the elastic bars. The purpose of this report is to analyze in detail many of the assumptions which must be made in order to draw meaningful conclusions from this technique.

This study has been prompted by a wide variety of conflicting statements which have recently appeared in the literature which challenge the validity of the split Hopkinson pressure bar technique. In particular, the results of a study of the dynamic properties of a high purity aluminum utilizing this technique were reported by Hauser, Simmons and Dorn [2]. They concluded that the aluminum tested not only exhibited a dynamic stress-strain relation but that the relation was a function of the rate of strain. However, various experimental analyses [3,4] of wave propagation in this material indicate that the rate independent theory of wave propagation developed by von Karman [5], Taylor [6] and Rakhmatulin [7] is adequate to predict its response. Bell [4] has recently reported an experimental study of the split Hopkinson pressure bar utilizing his diffraction grating technique on the specimen to obtain an independent measure of strain. Since a large difference in strain was observed between the direct measurement and that inferred from pressure bar measurements, Bell concluded that "...the source of the difficulty in the extended quasi-static impact tests lies in the assumption of uniform strain in the short elastically bounded specimen and in the neglect of wave propagation and interaction detail."

The effects of the wave propagation and interaction detail have been evaluated numerically in this report by applying the method of characteristics to the elastically bounded specimens.

---

*numbers in brackets designate references at end of report

In addition, the effects of friction and its resulting biaxial stress condition have been evaluated. Various experiments were performed at a variety of rates of strain in order to confirm certain assumptions. In all of the following analyses, the stress-strain relation of a material will be assumed to be unique in order to simplify the calculations. The response of the pressure bars is then calculated. In order to obtain the stress-strain relation of the specimen, the same assumptions may be employed as when the pressure bar response is obtained experimentally. The usual assumptions are as follows:

1. Uniform Axial Stress Distribution. If the specimen is made sufficiently short, it is assumed that the stress, and therefore the strain, is "effectively the same throughout the specimen." [8] This assumption is equivalent to neglecting the effect of axial inertia in the specimen.

2. Frictionless Interface. The presence of friction at the faces of the specimen will cause a combined stress situation to exist at the interface even in a "static" test which results in an "apparent" increase in stress for a given strain.

3. Uniform Radial Stress Distribution. This assumption effectively requires the radial stress to be zero and the axial stress to be constant across the diameter of the specimen.

4. The Boundary Conditions. Consistent with a one-dimensional analysis is the assumption that, at the interfaces between the specimen and pressure bars, the axial forces are equal.

The first two assumptions will be analyzed in detail in this report. The remaining assumptions will be the subject of a two-dimensional analysis in the near future.

WAVE PROPAGATION AND INTERACTION

The one-dimensional "rate insensitive" theory of finite amplitude wave propagation has been utilized to determine the transient response of the elastically bounded specimen in the split Hopkinson pressure bar experiment. The method of characteristics has been used to obtain a solution in the same manner as Conn [9]; however, the solution presented here has been carried to a logical conclusion which permits certain generalizations to be made regarding the effects of axial inertia. The approach taken here consists of assuming the stress in the specimen to be a known unique function of strain. For each incident strain pulse the wave interaction detail may be computed at any point in the specimen, as well as the reflected and transmitted strain pulses in the pressure bars. The assumptions outlined in the preceding section are invoked in order to obtain an "apparent" stress-strain relation which includes the effects of axial inertia. A comparison of the "apparent" and assumed stress-strain

relations indicates the error to be expected due to the existence of finite amplitude wave propagation.

The governing equations which describe the motion of the specimen and pressure bars, as well as the details of the computational technique, are contained in Appendix A. The calculation has been reduced to a systematic set of machine instructions, the CASH code (Appendix B), which permits the automatic computation of the entire characteristic net. The stress-strain relation of the specimen is assumed to be linearly elastic below, and parabolic above, the yield stress. However, a discontinuity in the slope of the curve is permitted at the yield stress so that a wide variety of materials are described by this representation.

Experimental Confirmation

Due to the many assumptions contained in this type of analysis, it is desirable to perform a calculation where experimental data are available. Therefore, one of the experiments on commercially pure aluminum recently reported by Bell [4], which is extremely well documented, has been used to demonstrate the accuracy of this computational technique as well as the non-dimensional nature of the one-dimensional solution. It is assumed that the specimen is linearly elastic to a stress of 1000 psi and the resulting stress and strain at yield is one point on a parabola. A second point on the parabola of Bell [4] at a stress of 25,000 psi has been used to obtain an adjusted parabola which when normalized with respect to the strain at yield is given by:

$$E = 0.66942 - 2.975207S + 3.305787S^2 \qquad (1)$$

This equation is presented in figure 1 where it is compared with the parabolic law given by Bell [4]. The "hard" aluminum pressure bars were assumed to be 2024-T6 having a modulus of 10^7 psi and a density of .1 lb/in^3. The same modulus and density were assumed for the specimen in the elastic region. The pressure bars were 1.0 inch in diameter and the specimen had an ℓ_o/d_o of $\frac{1}{2}$ and a diameter of 0.96 inch which closely approximates test no. 827 reported by Bell [4]. The data deck described in Appendix B for this case is given in Table 1.

The computed strains at the center of the specimen, as well as the computed average strains, are compared in figure 2 with experimental values reported by Bell [4]. Relatively good agreement is obtained between the computed strain and the average specimen strain obtained from pressure bar measurements. Since dry specimen-pressure bar interfaces were used for this test and the computation assumes perfectly lubricated interfaces, the deviation is well within the error to be expected. The radical departure of the diffraction grating measurements at approximately 4 percent strain is consistent with an experimental difficulty

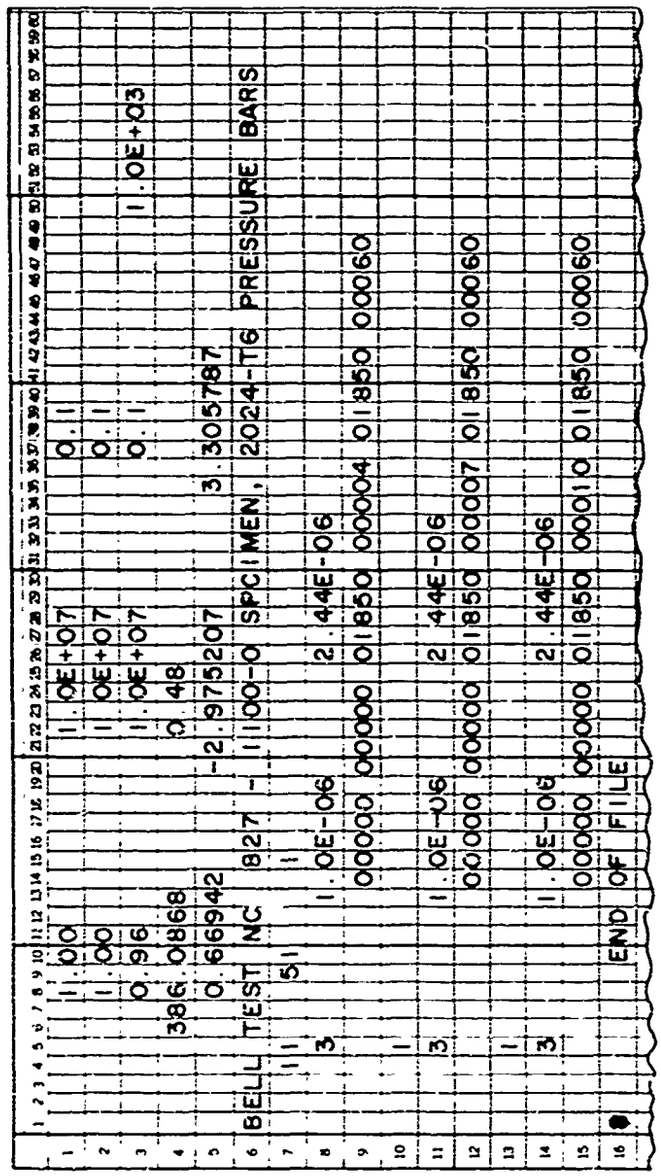

TABLE 1 CARD PUNCH LAYOUT

reported by Bell [10] subsequent to the publication of the data contained in figure 2. The difficulty is associated with a pronounced change in reflectivity of the surface at strains above 4.3 percent.

Axial Inertia Effects

The CASH code has been used in conjunction with the REDUCE code to evaluate the effects of wave propagation in the specimen on the "apparent" stress-strain curve. The REDUCE code is merely a machine program which is used to process the incident, reflected and transmitted strain records to obtain the "apparent" stress-strain curve. Although originally developed to process experimental data, it is directly applicable to the strain pulses computed by the CASH code.

In order to assess the various effects of axial inertia on the resulting "apparent" stress-strain curve, the results of the problem considered in the preceding section are presented in detail. The nonuniform strain distribution which is most severe during the earlier portion of the test is presented in figure 3(A) as a function of both time and position along the specimen. In addition, the difference in stress across the specimen, which is averaged in order to obtain the stress-strain curve, is presented in figure 3(B). It may be seen that the effect of nonlinear wave propagation in the specimen is to damp this stress difference which oscillates about the origin. The "apparent" stress-strain curve is presented in figure 4 with the assumed stress-strain behavior superimposed for comparison. It should be noted that the "apparent" stress-strain curve is a reasonable approximation of the assumed stress-strain behavior for strains greater than 1.5 percent. The "apparent" overstress occurring at strains below 1.5 percent is an axial inertia effect and should not be confused with the initial overstress which occurs during the impact of a projectile against a target rod. This latter effect is caused by the initial three-dimensional behavior while the waveform is established in the target. The distortion of the "apparent" stress-strain curve is sufficient to preclude the determination of the yield stress or modulus for the case considered.

It has been found that the duration of this initial overstress is approximately twice the rise time of the incident strain pulse. Therefore, great care must be exercised in analyzing split Hopkinson bar data obtained during the time required to establish the initial uniform strain distribution in the specimen. This problem is alleviated somewhat if the material being tested has a well-defined yield stress such as work-hardened commercially pure aluminum. The case of work hardening to a yield stress of 11,000 psi as tested by Hauser, et al [2], and analyzed by Conn [9] has been considered. The assumed and computed stress-strain curves are presented in figure 5. Since the slope of the curve in the plastic portion of this material is much less than in the previously considered material, relatively large nonuniform strain

distributions may exist in the specimen with a much reduced effect on the stress distributions. Therefore, a good approximation of the yield stress may be obtained if there is a sharp discontinuity in the slope of the curve at that point.

The "acoustic impedance" of a rod is defined as:

$$I = \rho_o c A_o \qquad (2)$$

It has been found that the ratio of the pressure bar impedance to the specimen impedance, R, is a sensitive measure of the constancy of the specimen strain rate. The impedance ratio was varied by using steel, titanium and aluminum pressure bars in conjunction with various specimen geometries. Figure 6 illustrates the effect of this ratio on the average specimen strain rate. The wave speed required to compute the impedance is the plastic wave speed which is a function of time. Therefore, the material described by equation (1) was assumed in all cases and the wave speed at a stress of 10,000 psi was assumed constant to obtain the values of R given in figure 6. Since this ratio enters the calculation as a single quantity in the boundary conditions (Appendix A), it is reasonable to expect that a reduction in specimen diameter has the same effect as increasing the density of the pressure bars. This is reflected in figure 6 by the results for ratios of 15.4 and 14.8. The former are the results for aluminum pressure bars and a specimen to pressure bar diameter ratio of 0.72 while the latter are the results for titanium bars and a diameter ratio of 0.96.

It has been shown that the effect of averaging the end face strains will yield an "apparent" stress-strain curve which is a good approximation of the assumed behavior for times greater than twice the rise time of the incident strain pulse. However, if instead of averaging the pressure bar measurements, the stress is assumed to be constant, then the transmitted strain pulse is proportional to the average specimen stress and the reflected strain pulse is proportional to the average specimen strain rate. The effect of axial inertia on this type of data reduction is illustrated in figure 7 for an aluminum specimen described by equation (1) with an ℓ_o/d_o of unity. The oscillation of the curve about the assumed behavior is exaggerated because of the increased length of the specimen. Therefore, this type of data reduction is only useful when the difference in the stress across the specimen is small with respect to the average stress. Otherwise, a significant error could be introduced into the "apparent" stress-strain behavior if an attempt is made to average the resulting urve.

FRICTION ANALYSIS

The analysis contained in the preceding section is only valid in the absence of frictional forces at the interfaces between the specimen and pressure bars. However, compression testing of small cylinders, as shown in figure 8(A), at any speed is extremely difficult since the combination of friction and specimen length will cause a nonuniform stress distribution to exist near the ends. These "end effects" will give rise to two conditions which are experimentally observable; namely, (a) an increase in the force required to obtain a given deflection, and (b) a distortion of the specimen commonly referred to as "barreling."

The first of the experimental observables previously mentioned will be manifested in an "apparent" increase in stress to obtain the same strain. The following approach is based primarily on the analysis reported by Jackson and Waxman [11]. The magnitude of this effect can be estimated by assuming the presence of a shear stress which is proportional to the axial stress on each face of the specimen. The constant which expresses the ratio of the shearing stress to the axial stress is defined as the "coefficient of friction" and is given by the symbol μ. The differential equation which expresses the static equilibrium of forces shown in figure 8(B) is given by:

$$\frac{d\sigma_r}{dr} + \frac{\sigma_r - \sigma_\theta}{r} + 2\mu \frac{\sigma_z}{\ell} = 0 \tag{3}$$

If the material is assumed to be incompressible in the plastic regime, and if the Tresca yield criteria and Hencky-Mises flow law are employed, it can be shown [12] that:

$$\sigma_z = \sigma_o e^{2\mu(a-r)/\ell} \tag{4}$$

The resulting nonuniform stress distribution given by equation (4) is shown in figure 8(C). In order to determine the effect of such a stress distribution on the "apparent" stress-strain curve obtained from a compression test with friction, the force must be determined as a function of specimen geometry. The axial force for any given length is given by:

$$F_z = 2\pi \int_0^a \sigma_z \, r dr \tag{5}$$

If the "apparent" stress is defined as:

$$\sigma_a \equiv F_z/\pi a^2 \tag{6}$$

it can be shown that:

$$\sigma_a/\sigma_o = 2\alpha^{-2}\left[e^{\alpha} - (1+\alpha)\right] \tag{7}$$

where

$$\alpha = \beta(1+\epsilon)^{-3/2} \tag{8}$$

Here β is the ratio of the coefficient of friction to the original ℓ_o/d_o of the specimen and ϵ is the "engineering" strain.

The increase in "apparent" stress as a function of strain given by equation (7) is presented in figures 9 and 10 for various values of the parameter β of practical interest. Figure 9 demonstrates the error to be expected if cylinders with an original length to diameter ratio on the order of unity are compressed without lubricating the anvils. However, even when great care is taken to maintain a frictionless interface with lubricants such as molybdenum disulfide ($\mu = 0.04$), compression of short cylinders with an $(\ell_o/d_o) \approx .25$ could result in errors in excess of 5 percent.

Associated with the end effects of a short cylinder is the distortion of the specimen commonly referred to as "barreling." This is a two-dimensional effect which could cause erroneous results if stresses and strains are deduced from force and crosshead displacement measurements. However, a two-dimensional analysis by Davis and Jackson [13] was compared with the preceding analysis and revealed no significant differences at strains below 15 percent [12].

In order to confirm the validity of the one-dimensional analysis, several experiments were performed using commercially pure aluminum. A single rod of 1100-F aluminum as received was cut into one-foot lengths, heated to 650°F for 2½ hours, and oven cooled. All specimens used in this study were machined from this one piece of stock. Cylindrical compression specimens were machined with various ratios of length to diameter as listed in Table 2. One specimen was re-annealed at 650°F for 2½ hours so that the effects of residual stresses due to machining could be evaluated. The faces of each specimen were polished with emery cloth, cesium oxide and jewelers rouge, in that order. A pair of compression plates of 4340 steel, ground to a number three finish, were attached to a standard Baldwin-Southwark, 60,000-pound capacity, universal testing machine. The crosshead velocity of this machine was maintained at the constant values indicated in Table 2 in order to maintain the same constant strain rate for the various geometries. A lubricant consisting of molybdenum disulfide in a light oil solution was used throughout this series of tests.

Specimen	Length (in)	Diameter (in)	ℓ_o/d_o	β	Speed (in/sec)	$\dot{\varepsilon}$ (sec^{-1})
1	0.9862	0.4035	2.29	.072	1.65×10^{-3}	1.8×10^{-3}
2	0.9254	0.4277	2.16	.077	1.65×10^{-3}	1.8×10^{-3}
3	0.9270	0.4430	2.08	.080	1.65×10^{-3}	1.8×10^{-3}
4	0.9268	0.3820	2.36	.070	1.65×10^{-3}	1.8×10^{-3}
5	0.9264	0.3635	2.55	.065	1.65×10^{-3}	1.8×10^{-3}
6	0.9264	0.3425	2.70	.062	1.65×10^{-3}	1.8×10^{-3}
7	0.4633	0.3816	1.21	.137	1.65×10^{-3}	3.6×10^{-3}
8	0.4618	0.4444	1.04	.160	1.65×10^{-3}	3.6×10^{-3}
9	0.2320	0.4428	0.525	.316	1.65×10^{-3}	7.2×10^{-3}
10	0.2310	0.4243	0.547	.304	4.16×10^{-4}	1.8×10^{-3}
11	0.2300	0.4238	0.544	.305	4.16×10^{-4}	1.8×10^{-3}
12	0.1173	0.4238	0.277	.600	4.16×10^{-4}	3.5×10^{-3}

Table 2. Low Rate Testing - Specimen Configurations and Test Conditions

Specimen no. 1 was loaded to a stress of 11,000 psi, unloaded, re-lubricated, and then reloaded to a higher stress. This procedure was repeated several times to obtain the data presented in figure 11. The data were obtained by simultaneously recording the outputs of the internal balance of the testing machine and an electrical deflectometer attached to the crosshead of the machine which was assumed rigid. Specimen no. 2 was compressed to the same final strain as specimen no. 1 without re-lubricating during the test. The results of this test were identical to those illustrated in figure 11, indicating that lubrication was maintained throughout the test. Specimen no. 3 was re-annealed and tested with identical results indicating the lack of any significant residual stresses due to machining. Therefore, all remaining tests were performed without re-annealing or re-lubricating the specimens during the experiment. The remaining specimens were tested and the "apparent" stress-strain curves for length to diameter ratios from 2.70 to 0.277 were obtained.

The force-deflection data collected in this series of experiments are presented in figure 12 for three representative ratios of length to diameter. The discontinuities in the stress-strain behavior were repeatable and indicate that the material considered in this report is mechanically unstable. This observation is consistent with that reported by Kenig [14] where the stress-strain data were in the form of a staircase function instead of a smooth curve.

In order to determine the stress-strain relation for a frictionless test, and to assess the accuracy of the one-dimensional theory, it is noted that the exponential in equation (7) may be represented as a series:

$$e^{\alpha} = 1 + \alpha + \frac{\alpha^2}{2!} + \frac{\alpha^3}{3!} + \ldots . \qquad (9)$$

Substitution of this expression into equation (7) and neglecting higher order terms yields:

$$\sigma/\sigma_o = 1 + \alpha/3 \qquad (10)$$

Therefore, for a given value of strain the apparent increase in stress is inversely proportional to the original ratio of length to diameter of the specimen. This may be expressed as:

$$\frac{\sigma_1 - \sigma_o}{\sigma_2 - \sigma_o} = \frac{\alpha_1}{\alpha_2} = \frac{\beta_1}{\beta_2} = \frac{(\ell_o/d_o)_2}{(\ell_o/d_o)_1} \qquad (11)$$

Therefore, the stress to be expected from a frictionless test is given by:

$$\sigma_o = \frac{(\ell_o/d_o)\sigma_1 - (\ell_o/d_o)\sigma_2}{(\ell_o/d_o)_1 - (\ell_o/d_o)_2} \tag{12}$$

Inserting the values of σ_1 and σ_2 for ℓ_o/d_o's of 2.7 and 0.545, respectively, from figure 12 at 10 percent strain, it is found that:

$$\sigma_o = \frac{(2.7)(15,480) - (.545)(17,050)}{(2.7) - (0.545)} \text{ psi} \tag{13}$$

or

$$\sigma_o = 15,080 \text{ psi} \tag{14}$$

The "apparent" increase in stress for an ℓ_o/d_o of .545 is 13.05 percent at a strain of 10 percent. The value of β which will cause this increase may be determined from figure 9 and is found to be equal to 0.305. The coefficient of friction may then be computed from the definition of β and is found to be 0.166. The values of β for each test have been computed for this coefficient of friction and are tabulated in Table 2. A computed stress-strain curve for β equal to zero may be calculated from the data obtained with the maximum ℓ_o/d_o (specimen no. 6) corrected according to equation (7). The "apparent" stress-strain curves predicted by the one-dimensional analysis are illustrated in figure 12. Excellent agreement is obtained with the intermediate values of β and good agreement with the maximum value of β considered. The maximum deviation of the computed stress from that observed experimentally is 3.65 percent.

These results indicate that the effects of friction and specimen geometry cannot be considered independently, but will occur in a predictable manner. In addition, the measurement of crosshead displacement is an acceptable method of obtaining specimen strain when the effects of friction are small enough to preclude barreling. Although these results have been derived for a statically applied load, it will be assumed that the effects of friction and specimen geometry are synonymous dynamically, as well. It has also been demonstrated experimentally that even when great care is taken to eliminate friction, the use of relatively short specimens will introduce an "apparent" increase in stress very similar to reported strain rate effects. Therefore, the effects of friction should not be neglected unless it can be shown that the geometry of the specimen can be changed without affecting the resulting stress-strain curve when derived from load and deflection measurements.

EXPERIMENTAL EVIDENCE OF DYNAMIC BEHAVIOR

If the material under investigation is sensitive to the rate of loading, a radically different response may be indicated if these data are compared with the data obtained from low-speed testing such as that presented in the preceding section. However, since the rates of strain differ by approximately six orders of magnitude, such differences are entirely possible. In order to demonstrate that this different response is a property of the material and not due to the presence of friction, axial or radial inertia, dynamic data were obtained for commercially pure aluminum by two completely independent test techniques. Medium strain rate data were obtained with the more conventional high-speed testing equipment while high strain rate data were obtained with the split Hopkinson pressure bar technique. Although the strain rates produced by each technique do not overlap, they do provide data for a wide variety of strain rates.

Medium Rate Testing

The first series of experiments to be described was tested with the high-speed testing equipment shown in figure 13. This apparatus consists of a modified Plastechon Model 581 testing machine equipped with a Schavitz-Bytrex Model PL 2500 load cell, and an Optron Model 680AX electro-optical extensometer. The extensometer consists of two optical tracking units which generate an electrical signal proportional to the displacement of the target being tracked. The targets used in this series of tests were attached to the upper and lower faces of the compression cage shown in figure 13. The differential output of the two trackers is a voltage proportional to the "engineering" strain as a function of time. The frequency response of the extensometer is reported by the manufacturer to exceed 5 kc. The frequency response of the load cell-extension arm-compression cage combination has been determined experimentally to be 200 cps; however, calibration of both measuring devices was accomplished statically. The output of both the load cell and extensometer were recorded simultaneously and independently with a Tektronix Model 502A dual beam oscilloscope. The data taken during these tests were obtained with crosshead velocities sufficiently low to preclude the existence of axial or radial inertia effects in the specimens and/or "ringing" of the measuring or recording equipment.

The high-speed testing machine operates as shown schematically in figure 14. A high pressure nitrogen source provides a constant pressure to a piston which initially compresses the oil. By activating a solenoid valve the fluid is allowed to discharge through an orifice which is adjusted to obtain various constant crosshead velocities. The compression cage is fitted with a slack adapter which permits the crosshead to accelerate to a constant velocity prior to engaging the specimen.

Three specimens were machined from the same stock used for the "static" testing program. The dimensions of each specimen were identical (see the following table), and the same lubricant as used in the "static" tests was used to insure that any differences in observed stress could not be attributed to frictional effects. The crosshead velocity of each test was varied in order to achieve the variation in strain rate indicated in the following table. The data obtained from a typical test are presented in figure 15 as well as the stress-strain curves for the three rates of strain considered. The stress-strain curve derived in the preceding section for β equal to zero also is illustrated in figure 15. The data obtained from specimen no. 15 were not at constant strain due to the inability of this type of equipment to maintain a constant velocity at high rates of loading.

Medium Rate Testing - Specimen Configurations and Test Conditions

Specimen no.	Length (in)	Diameter (in)	ℓ_o/d_o	Speed (in/sec)	$\dot{\epsilon}$ (sec^{-1})
13	0.500	0.252	1.98	1.15×10^{-2}	.023
14	0.501	0.251	1.99	8.75×10^{-2}	.175
15	0.500	0.251	1.98	0.5 to 1.5	1. to 3.

Description of Split Hopkinson Bar Apparatus

The general arrangement of the apparatus used in this series of tests is similar to that used by Krafft, et al [15], Lindholm [16], and more recently by Tanaka, et al [17]. This apparatus is illustrated schematically in figure 16. The pressure bars were mounted on four Teflon V-blocks which were originally aligned by bore sighting from the high pressure section of the projectile launcher. Both pressure bars were machined from the same rod to insure the same properties and then ground to the same diameter as the projectile (0.483 inch). The material used was 7Al-4Mo titanium which has a yield stress certified to exceed 172,000 psi. Each pressure bar was instrumented with a pair of Micro-Measurements foil strain gages (type EA-06-125AD-120) diametrically mounted with an Eastman 910 adhesive for strain gage applications. At each strain measuring station the gages were wired to opposite arms of a Wheatstone bridge which causes the change in resistance of each gage due to axial strain to be additive and that due to bending to cancel. The output of these bridges is recorded by means of two Tektronix Model 531 oscilloscopes and cameras. The incident pressure bar was instrumented with a MicroSystems semiconductor strain gage (type PA3-16-120) located one inch from the impact point. The signal from this gage was used to trigger two delay units which were used to trigger the recording equipment at a suitably delayed time. Both pressure bars were 36 inches in length and the strain measuring station on

each pressure bar was located 18 inches from the specimen so that the simplified method of data reduction introduced by Lindholm [16] could be utilized. Integration of the reflected strain pulse was accomplished by means of a Tektronix Type "O" operational amplifier plug-in unit. The output of this amplifier was used to drive the horizontal sweep of a Tektronix Model 531 oscilloscope while the transmitted strain signal provided the simultaneous vertical deflection. The calibration of the Wheatstone bridges, operational amplifier and elastic wave speeds is described in detail in Appendix C.

A rectangular stress wave is generated by the impact of a titanium projectile launched from a small bore air gun. The projectile used was 10 inches in length which provided a pulse duration of approximately 100 microseconds as illustrated in figure 17. It may be seen that a rise time of approximately 4 microseconds is possible with the impact of a flat nosed projectile. However, the resulting oscillations which are introduced due to the finite diameter of the bar are undesirable for several reasons. The oscillation of the incident strain pulse will cause an oscillation in the particle velocity at the incident face of the specimen. This condition would cause a small amount of nonuniform work hardening on one side of the specimen. Since the effect of cyclic work hardening on the dynamic behavior of a material is not entirely clear [16], it should be avoided if at all possible. In addition, the averaging of this oscillation is only valid to obtain the force that generated the variation in strain and not the effect at the specimen end of the incident pressure bar.

In order to reduce this oscillation as much as possible the impact face of the projectile was rounded off to a one-inch radius. The incident strain pulse generated by this type of projectile is shown in figure 17(B) for a slightly lower impact velocity than that used to obtain figure 17(A). It should be noted that the rise time is increased to approximately 10 microseconds; however, the oscillation is attenuated as desired. Although the amplitude of this incident strain variation could be attenuated even more by increasing the diameter of the pressure bars, the variation of the reflected strain pulse would be amplified accordingly. In addition, the use of strain gages with relatively long gage lengths, which has been suggested, would only serve to hide this variation in strain and not eliminate it. Neither of the previously mentioned approaches were attempted to further reduce this oscillation.

Upon arrival of the incident pulse at the specimen, part of the wave is reflected back into the incident bar while part is transmitted. The transmitted wave propagates into the "throw-off" bar illustrated in figure 16, reflects from the free end and separates, just as the "measuring piece" in Hopkinson's original experiment. This technique prevents the specimen from being reloaded by any additional pulses, thereby permitting its recovery and measurement.

The specimens used in this series of experiments were again machined from the same stock of commercially pure aluminum previously described. Six different diameters and three different lengths, Table 3, were tested. The strain records obtained with specimen no. 19 are considered typical and are shown in figure 16. The same lubricant as used for the low-speed tests was used throughout this program. The change in original length of the specimen, while resulting in a variety of strain rates, was intended to demonstrate the lack of frictional effects under dynamic conditions.

As described by Lindholm [16], if it is assumed that the stress is uniform along the axis of the specimen, then the data may be reduced electronically as shown in figure 16. However, since this involves a needless additional assumption, the data have been reduced by computing the forces and particle velocities independently at each face of the specimen. The oscilloscope traces were "read" on a Universal Telereader Type 17A equipped with a Telecordex which automatically punches the resulting x-y coordinate information onto IBM cards. The three data decks (incident, reflected, and transmitted) are used as input to the REDUCE code which numerically determines the stress, strain rate and strain at each data point. This program also computes the difference in stress across the specimen in addition to the final stress-strain curve. The output of this program for specimen no. 19 is presented in figure 18.

Several important features may be seen by comparing the reduced data in figure 18 with the raw data in figure 16. The relatively small oscillation appearing on the reflected strain pulse gives rise to a significant oscillation in the reduced data. Since the frequency of this oscillation is predictable on the basis of geometric dispersion in the pressure bar [18], this variation in strain could have been eliminated prior to data reduction. However, the alternate method of retaining this variation in raw data and smoothing the reduced data was utilized. This problem is characteristic of the type of material being tested since the amplitude of such oscillations is very nearly proportional to the amplitude of the pulse being propagated [19]. As the strength of the specimen is increased, the amplitude of the reflected wave will decrease while that of the transmitted wave increases.

From figure 18 the average strain rate is seen to vary from 1450 to 900 sec^{-1}. If this material were sensitive to the rate of strain, this variation would have to be taken into account. One technique often employed is to cross plot stress as a function of strain rate for each value of strain. This requires several tests at a wide variety of strain rates to obtain the stress-strain curve at a constant strain rate. This was found to be unnecessary for the commercially pure aluminum tested.

The resulting stress-strain behavior of the specimen is illustrated in figure 18(C). Based on the results of the

Specimen	Length	Diameter	ℓ_o/d_o	$\dot{\epsilon}_{max} \times 10^{-3}$	$\dot{\epsilon}_{avg} \times 10^{-3}$	Final Length
16	0.463 in	0.448 in	1.03	1.43 sec^{-1}	1.10 sec^{-1}	0.403 in
17	0.233	0.443	0.525	2.69	1.88	0.188
18	0.116	0.445	0.261	5.39	3.39	0.077
19	0.464	0.4	1.09	1.45	1.10	0.399
20	0.232	0.4	0.548	3.14	2.23	0.175
21	0.116	0.424	0.273	5.84	3.76	0.073
22	0.463	0.402	1.15	1.71	1.35	0.373
23	0.238	0.404	0.590	2.34	1.68	0.190
24	0.117	0.403	0.291	5.25	3.28	0.079
25	0.464	0.382	1.21	1.71	1.34	0.370
26	0.234	0.382	0.612	3.50	2.59	0.156
27	0.116	0.384	0.302	5.88	3.79	0.073
28	0.463	0.364	1.275	*	*	0.370
29	0.233	0.364	0.640	3.30	2.46	0.162
30	0.115	0.364	0.316	6.40	4.14	0.066
31	0.465	0.342	1.36	1.84	1.50	0.352
32	0.231	0.344	0.674	3.28	2.55	0.152
33	0.116	0.343	0.335	4.77	3.31	0.077

* delayed trigger - data incomplete

Table 3. High Rate Testing - Specimen Configurations and Test Conditions

one-dimensional wave analysis the data collected during the first 20 microseconds (twice the rise time of the incident pulse) has been ignored. The oscillations predictable from geometric dispersion of the reflected pulse in the elastic pressure bar have been smoothed and the resulting curve superimposed on figure 18(C) for comparison.

In order to demonstrate that the increase in stress indicated by these experiments is independent of the specimen length, the stress-strain behavior of specimen no. 21 is compared with that of specimen no. 19 in figure 19. It is apparent that this material exhibits the same stress-strain response for rates of strain from 1000 to 4000 sec^{-1}. However, the data obtained from this series of experiments are relatively scattered and cannot be presented as a single curve or a family of rate sensitive curves. The variation in the stress-strain behavior of this material for this series of experiments is illustrated in figure 19 and is indicative of the level of confidence which should be placed in any dynamic results for this material.

Two techniques were used to independently verify the accuracy of these experiments. The specimen was recovered after each test, examined, and the final length determined. No evidence of barreling was observed and the final strain measurement was within one percent of the maximum strain indicated by the resulting stress-strain curve. Although this indicates that the specimen strain may be computed accurately from pressure bar measurements, it does not provide a verification of the stress measurement. Therefore, an energy balance was performed in an attempt to provide this verification. Applying the theory of one-dimensional elastic wave propagation, it was found that the energy absorbed by the specimen is given by:

$$\theta_s = E_p c_p A_p \int_0^\tau (\epsilon_I^2 - \epsilon_R^2 - \epsilon_T^2)dt \qquad (15)$$

where τ is the duration of the pulse. The energy absorbed by the specimen may be attributed to the sum of the strain and kinetic energies. The resulting unbalance in energy is then an estimate of the accuracy of the strain measurements. An increase in temperature of the specimen was computed assuming an adiabatic process and a specific heat at constant volume of 0.217 Btu/lb°F. Based on the results of Farren and Taylor [20] it has been assumed that 93 percent of the strain energy appears as a temperature increase. The results of this calculation for the data contained in figure 16 are listed in Table 4.

Although the temperature increase of 6.28°F indicates that the effect of thermodynamics on the resulting data is negligible for this particular specimen, it does not provide an independent check of the magnitude of the stress-strain relation obtained from this test since the same balance could be obtained with less strain energy and only a slight increase in internal energy.

Table 4. Energy Analysis of Specimen No. 19

	(in lb)	percent
Incident Strain Energy	122.85	
Incident Kinetic Energy:	122.85	
Total Incident Energy:	245.7	
Reflected Strain Energy:	48.65	19.8
Reflected Kinetic Energy:	48.65	19.8
Transmitted Strain Energy:	15.5	6.3
Transmitted Kinetic Energy:	15.5	6.3
Specimen Strain Energy: ($\Delta T = 6.28°F$)	104.0	42.3
Specimen Kinetic Energy:	0.06	-
Energy Unbalance (% Error)	13.4	5.5
Total Energy:	245.7	100.0

DISCUSSION OF RESULTS AND CONCLUSIONS

The analyses contained in this report have been performed in an effort to establish the limitations of the split Hopkinson pressure bar as a technique to obtain dynamic stress-strain relationships.

Axial Inertia Effects

In the analysis of results obtained from the split Hopkinson pressure bar it is assumed that the average stress and strain rate in the specimen at any time may be approximated by the average of the stresses and particle velocities of the end faces of the specimen. The effects of the large gradients of stress and strain caused by axial wave propagation in the specimen have been evaluated. Although certain conditions have been found where the nonuniformities of stress and strain are severe, the effect of the averaging process is to yield an "apparent" stress-strain curve which is a reasonably close approximation of the actual stress-strain behavior. Due to the finite rise time required to develop the incident strain pulse, a significant overstress will be apparent during the earlier portions of the test. Fortunately, this overstress is not an accumulative effect. However, modulus data cannot be obtained and yield stress can only be obtained approximately by this technique since both phenomena usually occur during this portion of the test when the averaging process is not valid. It has been found that as the ratio of the "acoustic impedance" of the pressure bar to that of the specimen is increased, the average rate of strain approaches a constant value. The effect of assuming a uniform stress and strain rate has been found to increase the amplitude of the oscillation of the "apparent" stress-strain curve about the actual curve. However, the average of this resulting curve again appears to be a good approximation of the actual behavior of the material.

End Effects

The effects of a shearing stress on the faces of the specimen have been examined statically, both theoretically and experimentally. It has been found that the effects of friction and specimen geometry cannot be considered independently. It has been shown that a reduction in the initial ℓ_o/d_o of a short compression specimen will have the same effect as an increase in the coefficient of friction for the same specimen geometry. It also has been demonstrated that "barreling" will be initiated at lower values of strain as the ratio of the coefficient of friction to the specimen ℓ_o/d_o is increased.

The effects of friction predicted by the one-dimensional analysis have been observed experimentally. Since the agreement between the predicted load-deflection behavior and that observed

experimentally is considered excellent, a method is presented whereby the actual or frictionless stress-strain behavior of the material may be computed.

Experimental Results

Load-deflection data have been obtained for annealed 1100-F commercially pure aluminum at room temperature and at rates of strain from 1.8×10^{-3} sec^{-1} to 6.4×10^{3} sec^{-1}. Low-speed or "static" testing indicates that the material under consideration is rate insensitive at the lower rates of strain. In addition, these tests indicate that commercially pure aluminum is a mechanically unstable material as defined by Kenig [14].

Reasonably good agreement with the frictionless low-speed test results was obtained with a medium rate testing machine at a strain rate of 2.3×10^{-2} sec^{-1}. However, a significant change in the stress-strain behavior was indicated as the rate of strain was increased to .175 sec^{-1} for the same specimen geometry. If the results obtained from the preceding friction analysis may be assumed valid at these velocities, then the increase in stress at a given strain may not be attributed to friction, or axial or radial inertia effects. It was observed that after an initial increase in stress, the data approached that given by the static response of this material.

Split Hopkinson pressure bar results have been obtained for this material at a variety of specimen geometries. It has been shown that for a given diameter, the length of the specimen may be reduced by a factor of four without significantly affecting the resulting stress-strain curve. This indicates that the effects of friction are insignificant at these rates of strain if the results of the static analysis are applicable.

Due to the scatter in data obtained for this material at rates of strain on the order of 10^{3} sec^{-1}, the values of stress illustrated in figure 20 for the split Hopkinson pressure bar are only considered accurate to ±5 percent. This relatively large scatter in data is considered to be indicative of a definite limitation of this test technique when applied to mechanically unstable materials. The recently reported phenomena of "catastrophic straining at one "point" in a specimen," [21] in annealed 1100 aluminum could easily render the dynamic testing of short specimens meaningless. This phenomena is a characteristic of the specimen and is not indicative of the accuracy to be expected from the split Hopkinson pressure bar technique with mechanically stable materials. Probably the best proof of the validity of this technique is its ability to determine that a stable material is insensitive to strain-rate; such as, 7075-T6 [22]. The dynamic behavior has been observed to be the same as the static relation with the split Hopkinson pressure bar technique.

Finite Amplitude Wave Propagation

An independent method of obtaining the dynamic stress-strain behavior of a rate insensitive material is available [23]. However, before considering the experimental observations it is necessary to clarify certain misconceptions which have developed over the past few years regarding the "rate independent" theory of plastic wave propagation.

It can be shown [12] that the same differential equations as those developed by von Karman are applicable to a rate sensitive material along certain paths, i.e.,

$$dv = \frac{d\sigma}{\rho_o c} \tag{16}$$

along

$$c = \pm\left\{\frac{(\partial\sigma/\partial t)}{\rho_o(\partial\epsilon/\partial t)}\right\}^{\frac{1}{2}} \tag{17}$$

If the stress is expressed as a function of strain and strain rate then:

$$\rho_o c^2 = \left(\frac{\partial\sigma}{\partial\epsilon}\right)_{\dot{\epsilon}} + \left(\frac{\partial\sigma}{\partial\dot{\epsilon}}\right)_{\epsilon} \frac{d \ln \dot{\epsilon}}{dt} \tag{18}$$

If the behavior of a material is insensitive to the rate of strain ($\partial\sigma/\partial\dot{\epsilon} \approx 0$) but still differs from the "static" behavior, then the measurement of finite amplitude wave speeds is an accurate measure of the slope of dynamic stress-strain curve at each level of strain. Therefore, the theory employed by Bell is completely justified and only the limitations of the experimental observations need be considered.

Two features must be demonstrated experimentally in order to assert that a material is insensitive to the rate of strain. First, it must be shown that the wave speed associated with each level of strain is a function of the strain alone. Second, it must be shown that the area under the predetermined wave speed-strain diagram will uniquely determine the particle velocity. The first condition may be demonstrated by relatively few experiments since each test contains strain values from zero to the maximum strain determined by the impact velocity. However, the second condition requires a separate test at each velocity for which the rate insensitivity is to be demonstrated. Unfortunately, this second condition is relatively insensitive to changes in the yield stress of the material because of the violent change in wave speed for very small values of strain. Therefore, in order to demonstrate rate insensitivity, the maximum strains developed for extremely low impact velocities would have to be measured.

It has been asserted by Bell [24] that the relationship

$$\int_0^{\epsilon_{max}} c \, d\epsilon = v_o \tag{19}$$

has been found to apply for impact velocities "from less than 100 in/sec to 3000 in/sec." However, since the amount of scatter in the data that had to be averaged to obtain these wave speeds does not appear in the literature, it is possible that the relationship:

$$v_D + \int_{\epsilon_D}^{\epsilon_{max}} c \, d\epsilon = v_o \tag{20}$$

would also satisfy the same experimental observations. If this is possible, then the resulting dynamic stress-strain relation could be found from the expression:

$$\sigma = \sigma_D + \rho_o \int_{\epsilon_D}^{\epsilon} c^2 \, d\epsilon \tag{21}$$

where σ_D is a rate sensitive stress occurring at a strain, ϵ_D, above which the material is rate insensitive. Therefore, the disagreement in the dynamic stress-strain behavior of a material obtained by the measurement of wave speeds does not invalidate the results obtained from split Hopkinson pressure bar experiments, but does demonstrate the rate insensitivity of the material for certain strains. These results are in agreement with recent experimental observations of Bodner and Clifton [25] who found the plastic deformation of commercially pure aluminum to be insensitive while the yield stress was sensitive to the rate of strain.

CONCLUSIONS

The analyses contained in this report permit the following conclusions regarding the validity of the split Hopkinson pressure bar technique:

1. Experiments utilizing finite amplitude wave propagation have not yet demonstrated the insensitivity of commercially pure aluminum at strains near the yield point and, therefore, do not contradict various split Hopkinson pressure bar results appearing in the literature.

2. The existence of nonlinear wave propagation in the specimen significantly affects the "apparent" stress-strain behavior of the specimen for a time equal to approximately twice the rise time of the incident strain pulse. As a direct consequence, it is unlikely that elastic modulus information

can be obtained by this technique for most metals. In addition, the yield stress can be only approximated, unless there is a distinct change in the slope of the stress-strain curve at the yield stress.

3. "Apparent" stress and strain levels obtained at later times by averaging pressure bar measurements are not significantly affected by nonuniform stress and strain distributions. The effects of friction are not evidenced in the "apparent" dynamic behavior observed.

4. Commercially pure aluminum has exhibited a dynamic behavior at rates of strain where axial and radial inertia effects are insignificant. However, split Hopkinson pressure bar results for this material are questionable due to an inordinate amount of scatter.

It is concluded that this technique for the determination of dynamic material behavior is capable of generating stress-strain relations with reasonable accuracy only in the region of gross plastic deformation for mechanically stable materials. Maximum usefulness in terms of constancy of strain rate and minimum oscillations will result from the use of high "acoustic impedance" pressure bars with a minimum diameter. Although the effects of friction do not appear to be as severe as in static testing, a lower limit on the specimen ℓ_o/d_o must exist and may be dictated more by radial inertia and adiabatic heating than interface friction. This is a problem which will require further study but does not affect the results contained in this report.

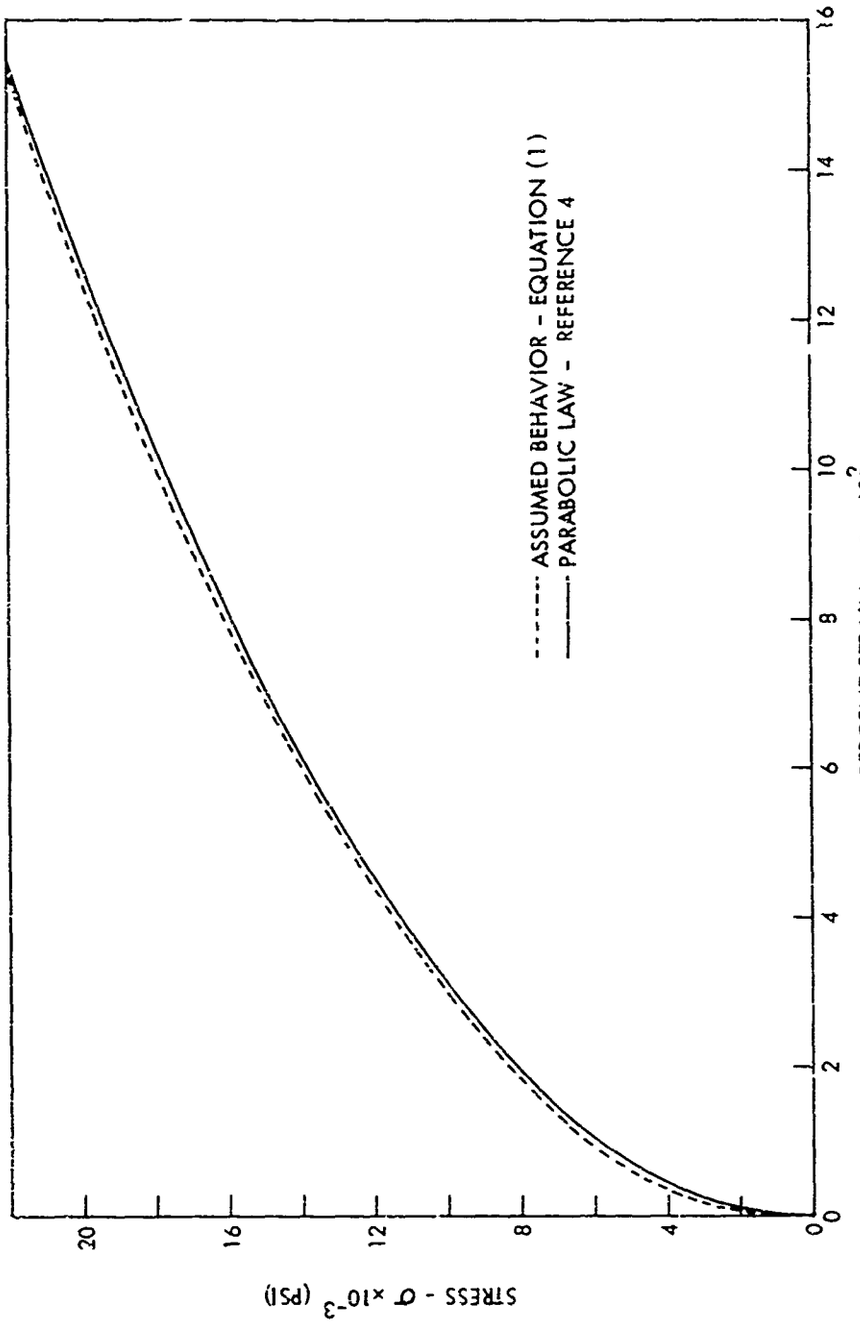

FIG. 1 STRESS-STRAIN BEHAVIOR OF COMMERCIALLY PURE ALUMINUM

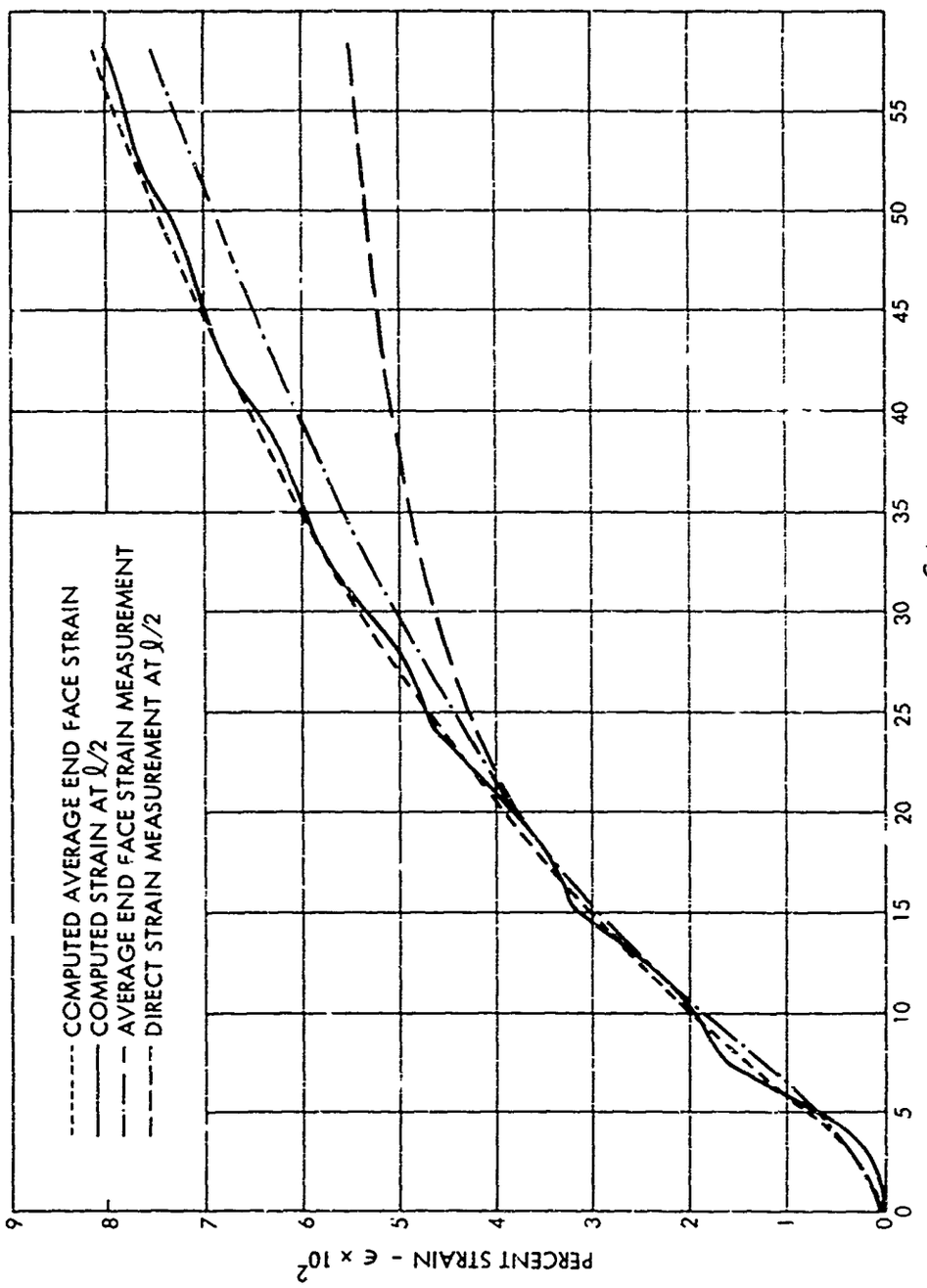

FIG. 2 CORRELATION OF CASH CODE WITH EXPERIMENTAL OBSERVATIONS

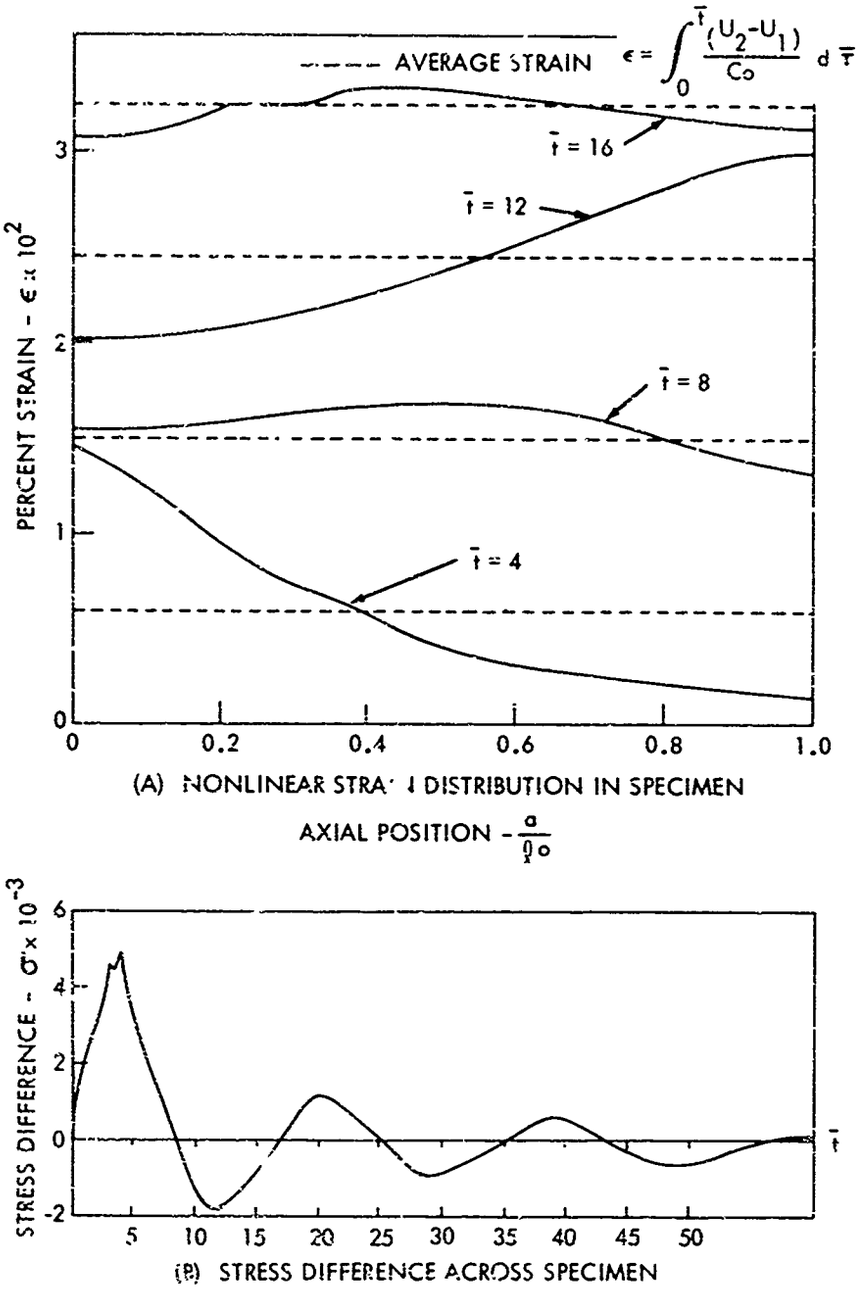

FIG. 3 EFFECTS OF AXIAL INERTIA ON STRESS AND STRAIN DISTRIBUTIONS

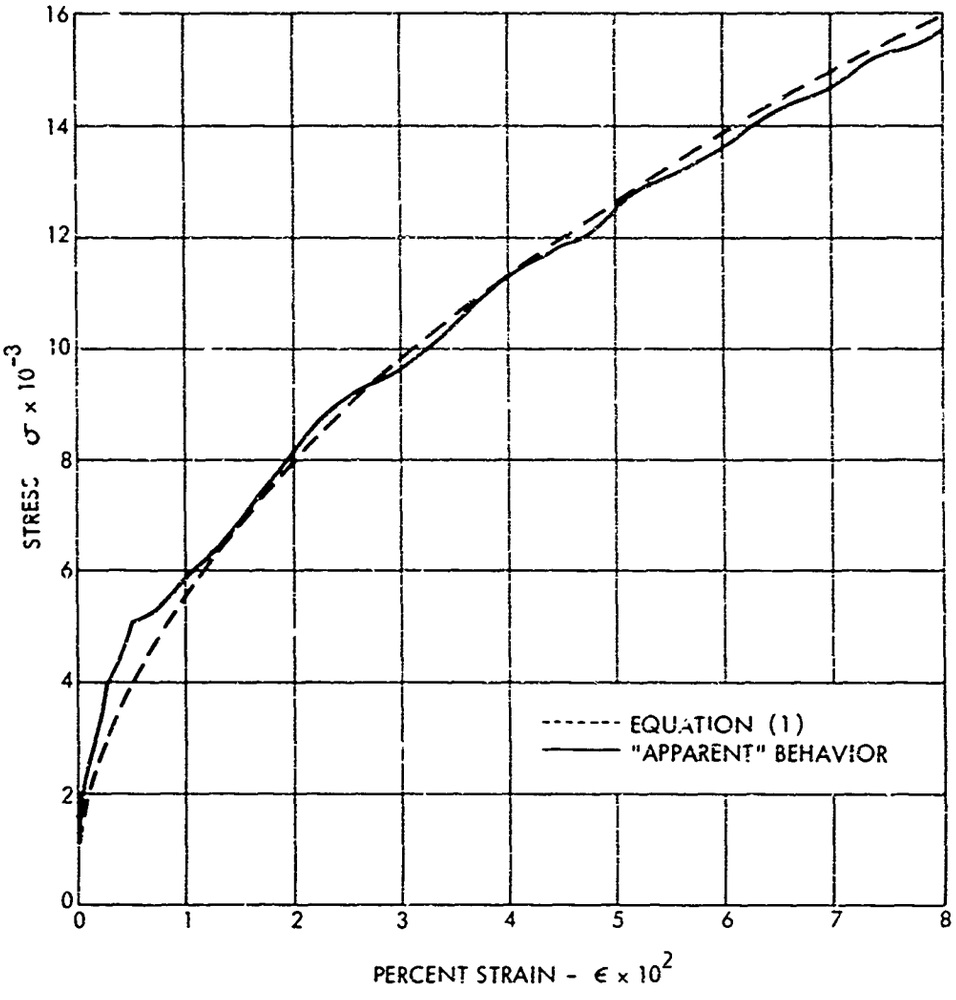

FIG. 4 COMPARISON OF ASSUMED AND "APPARENT" BEHAVIOR

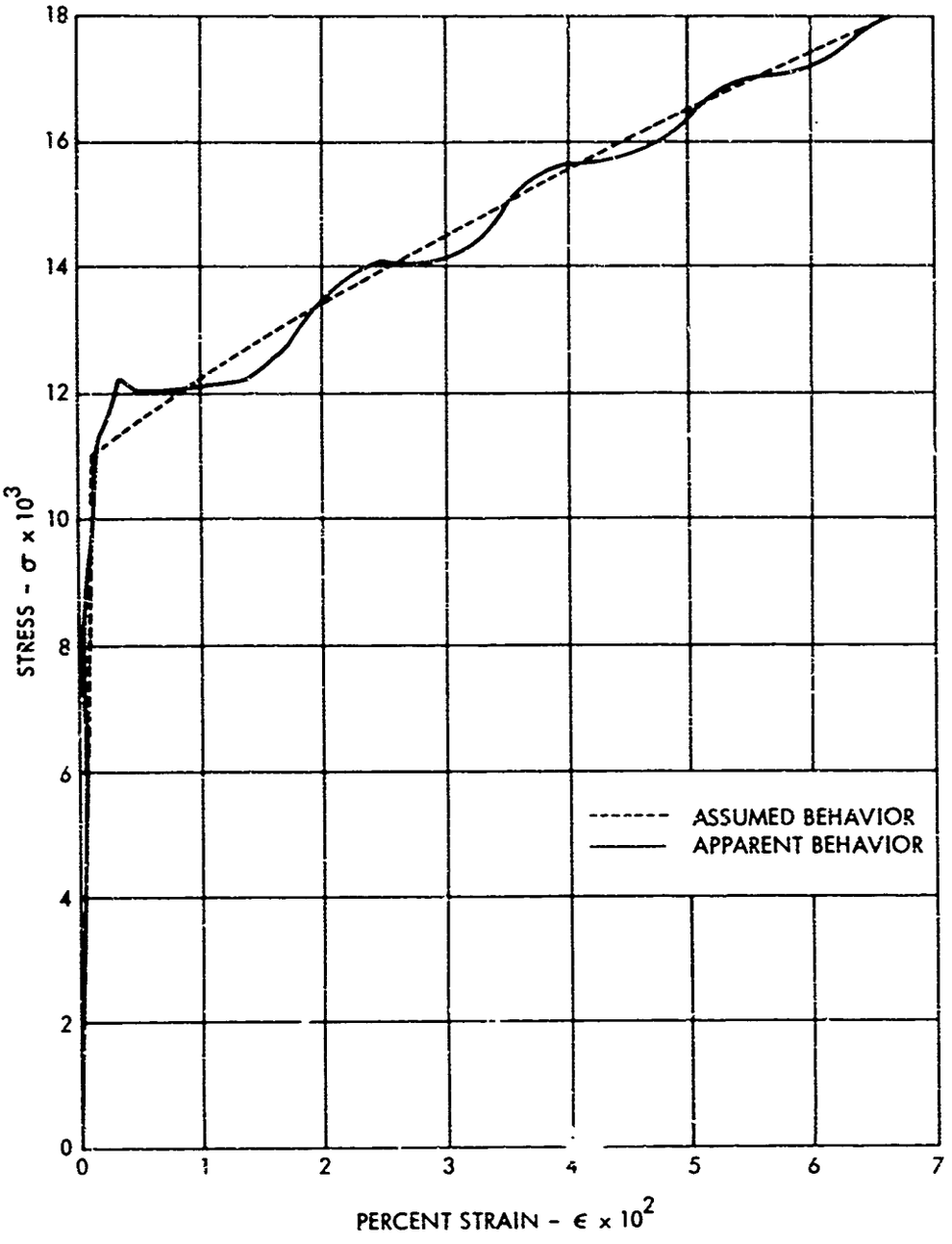

FIG. 5 EFFECT OF AXIAL INERTIA ON DISTINCT YIELD STRESS

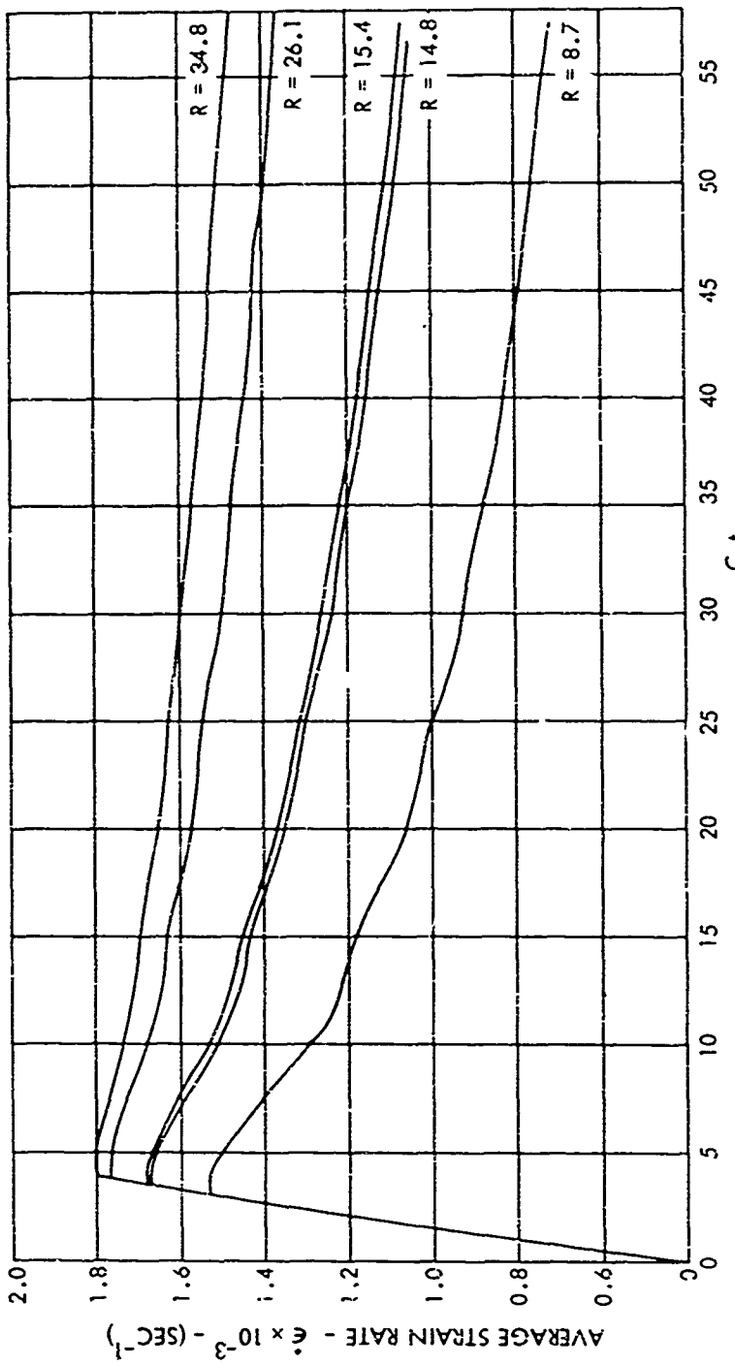

FIG. 6 EFFECT OF IMPEDANCE RATIO ON AVERAGE STRAIN RATE

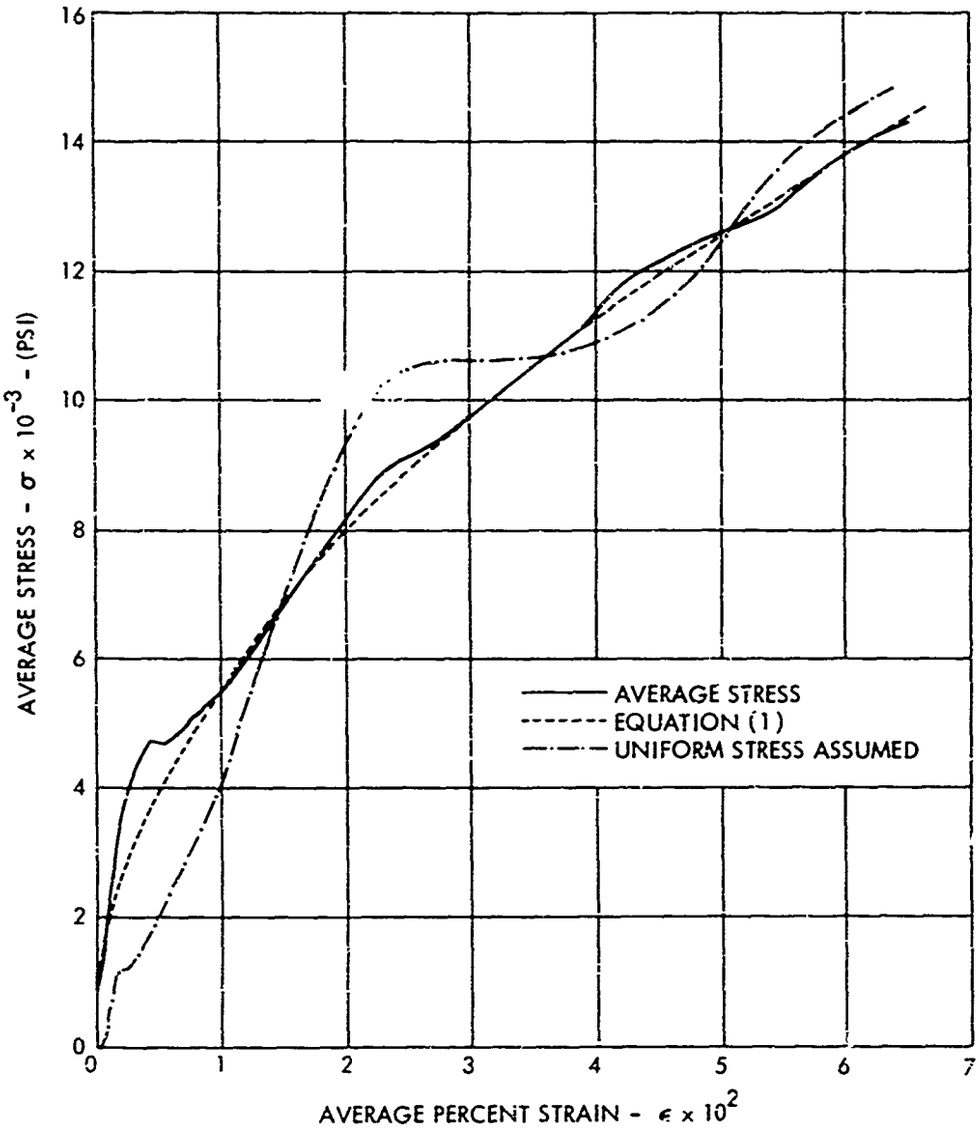

FIG. 7 EFFECT OF DATA REDUCTION ON APPARENT BEHAVIOR

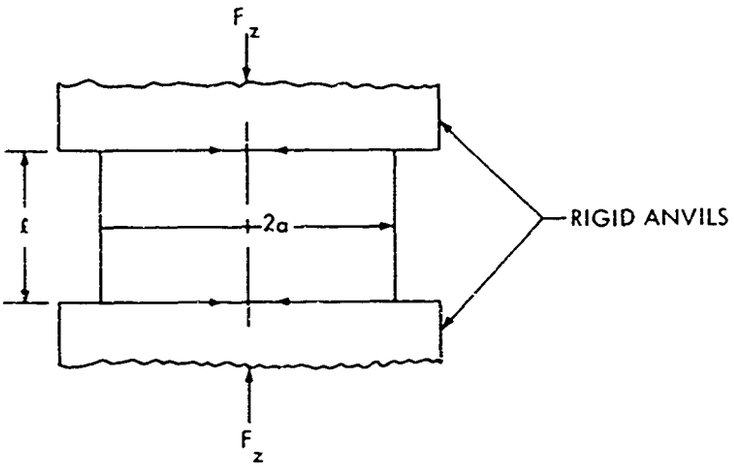

(A) SPECIMEN GEOMETRY

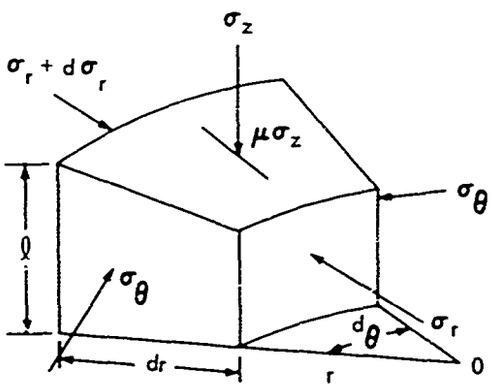

(B) DIFFERENTIAL ELEMENT OF SPECIMEN

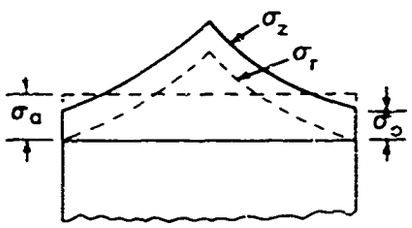

(C) STRESS DISTRIBUTIONS WITH FRICTION

FIG. 8 ONE-DIMENSIONAL FRICTION ANALYSIS

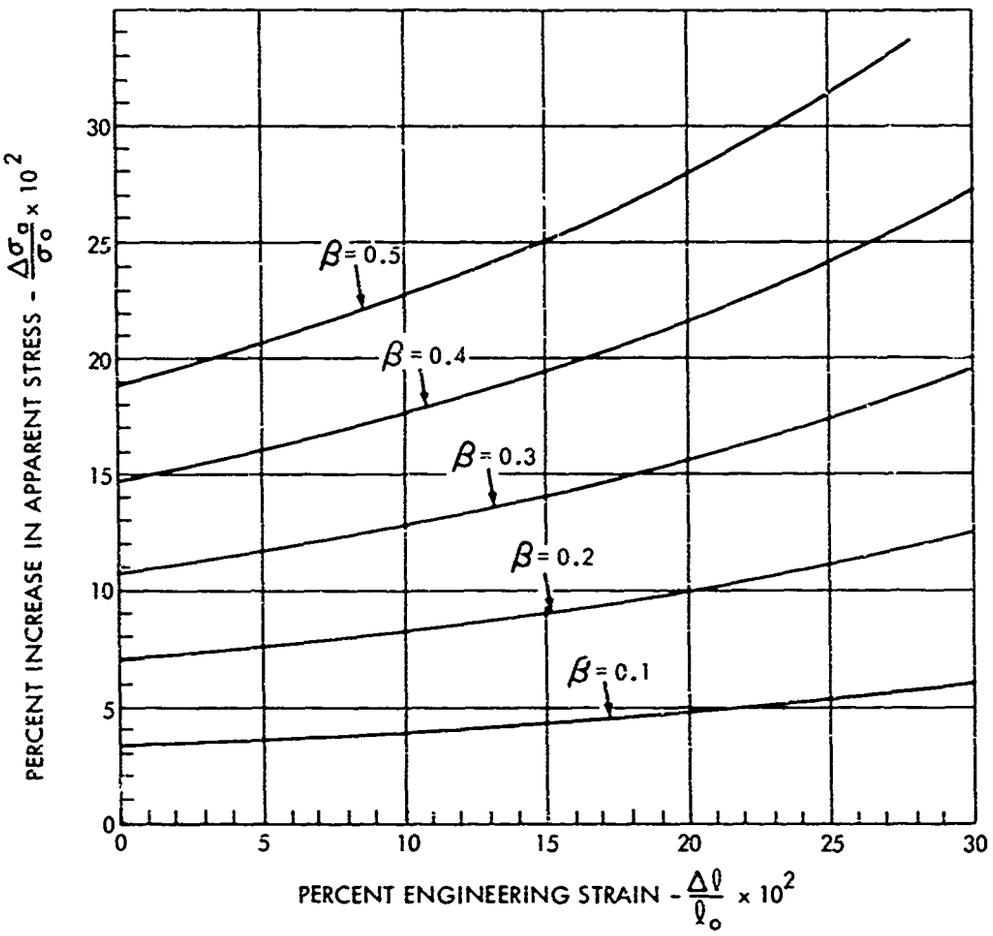

FIG. 9 ONE-DIMENSIONAL FRICTION EFFECTS ($0.1 < \beta < 0.5$)

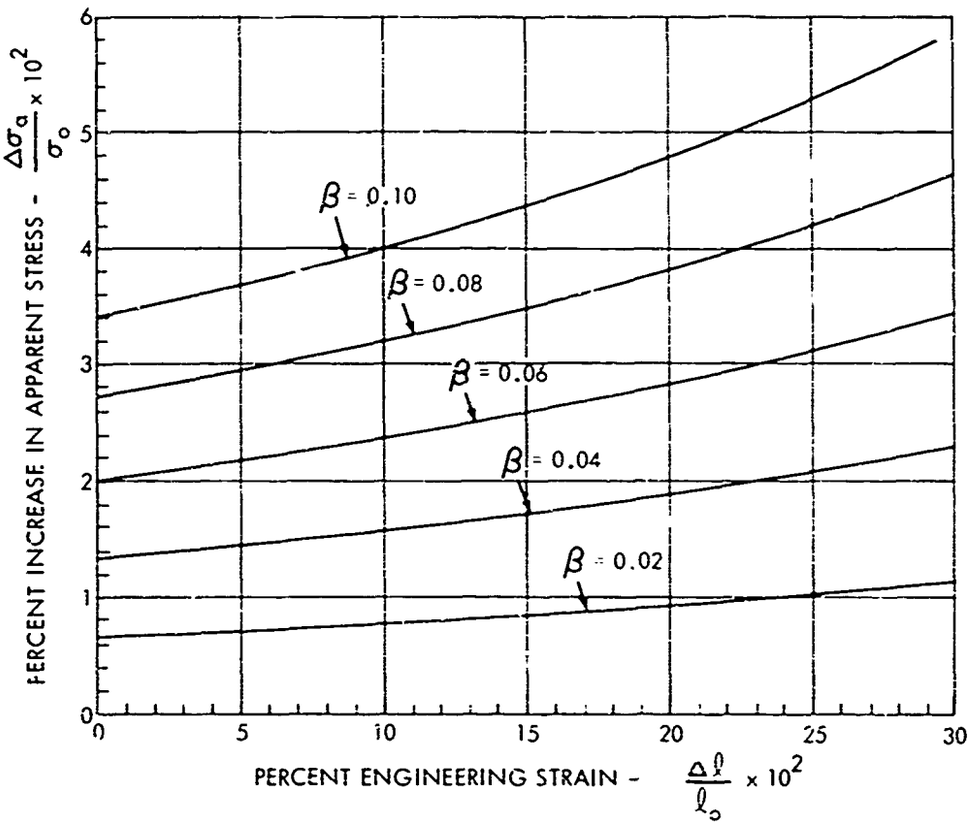

FIG. 10 ONE-DIMENSIONAL FRICTION EFFECTS ($0 < \beta < 0.1$)

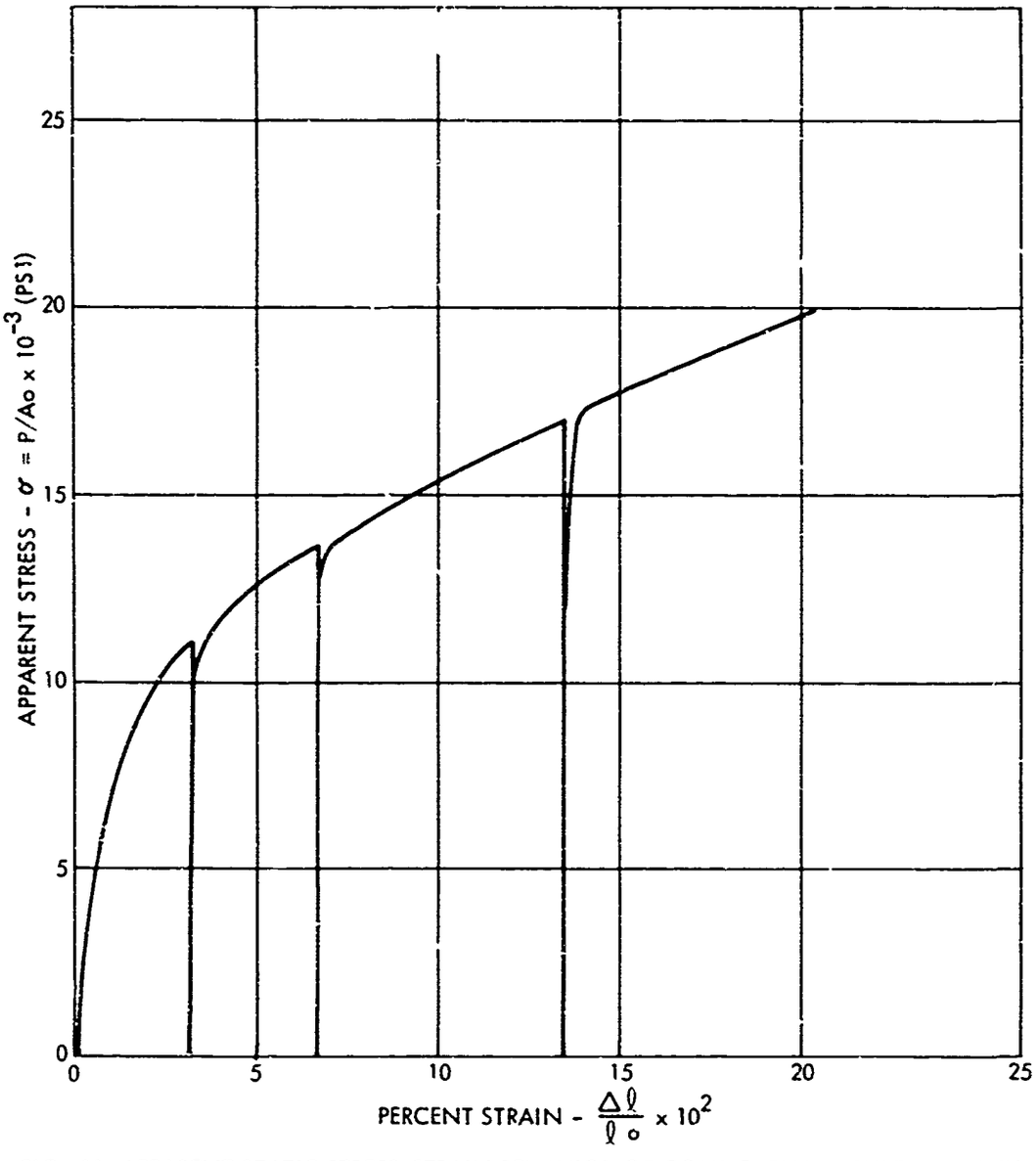

FIG. 11 APPARENT STATIC STRESS-STRAIN BEHAVIOR OF COMMERCIALLY PURE ALUMINUM

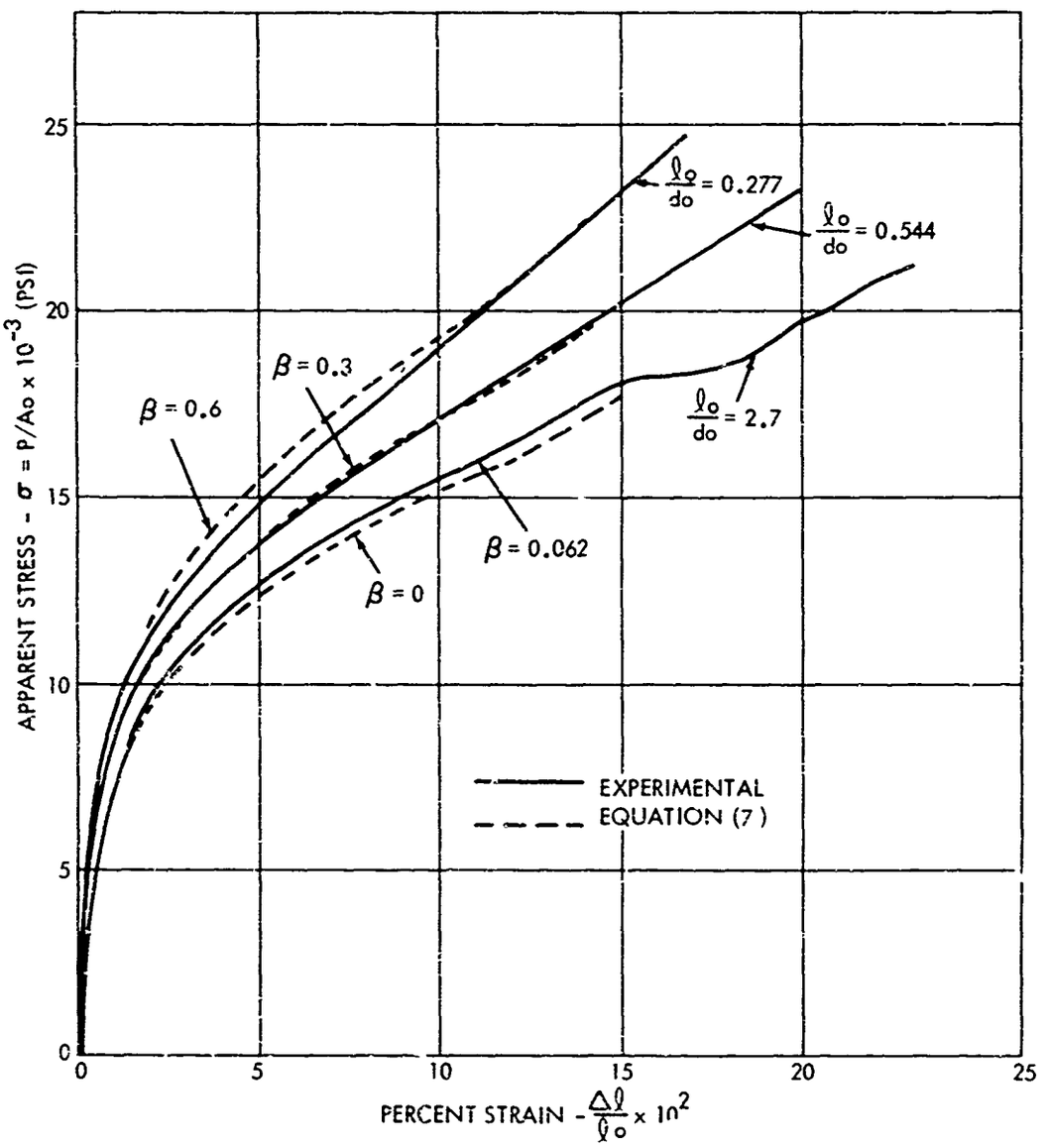

FIG. 12 EFFECTS OF FRICTION ON APPARENT STRESS-STRAIN BEHAVIOR

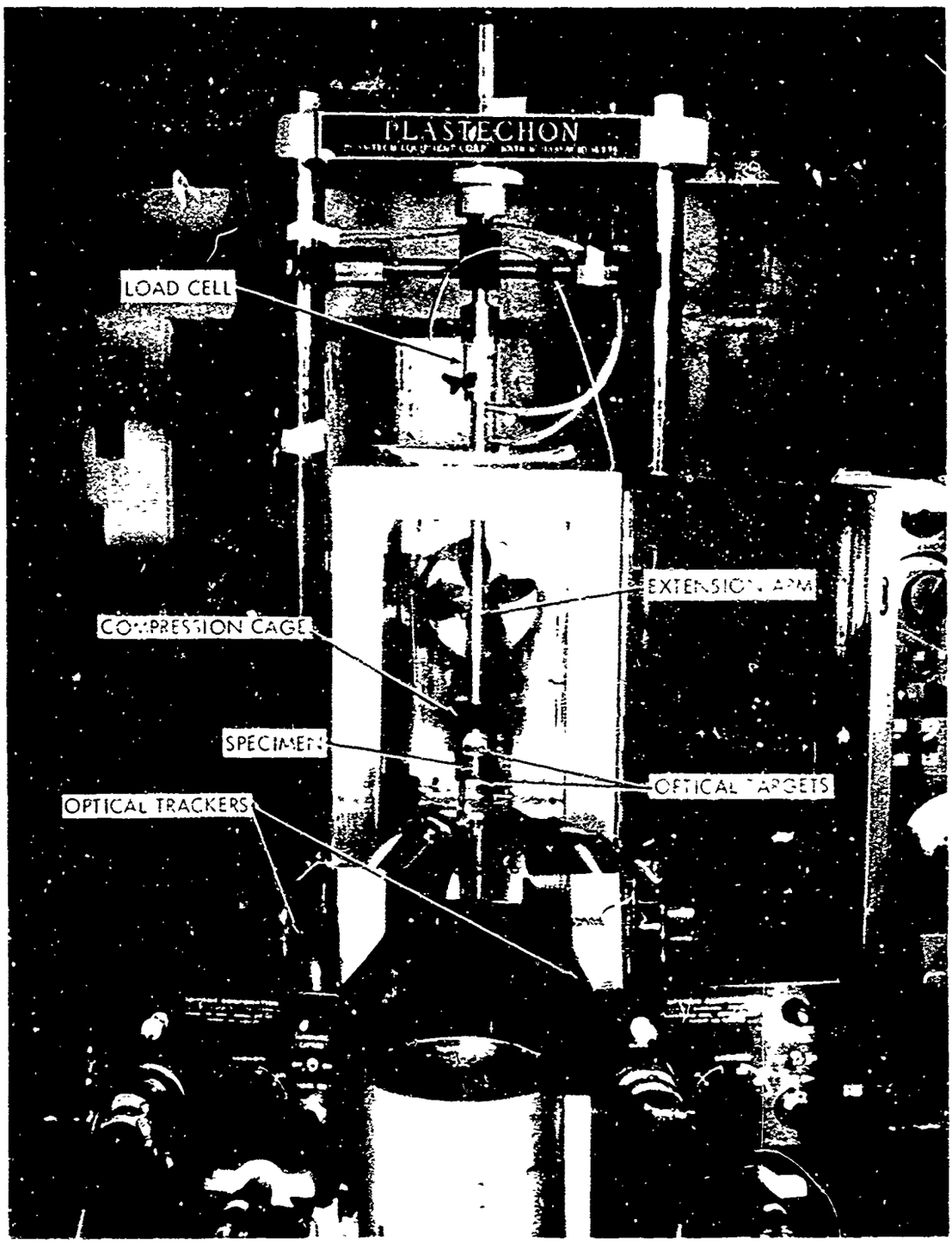

FIG. 13 MEDIUM RATE TESTING APPARATUS

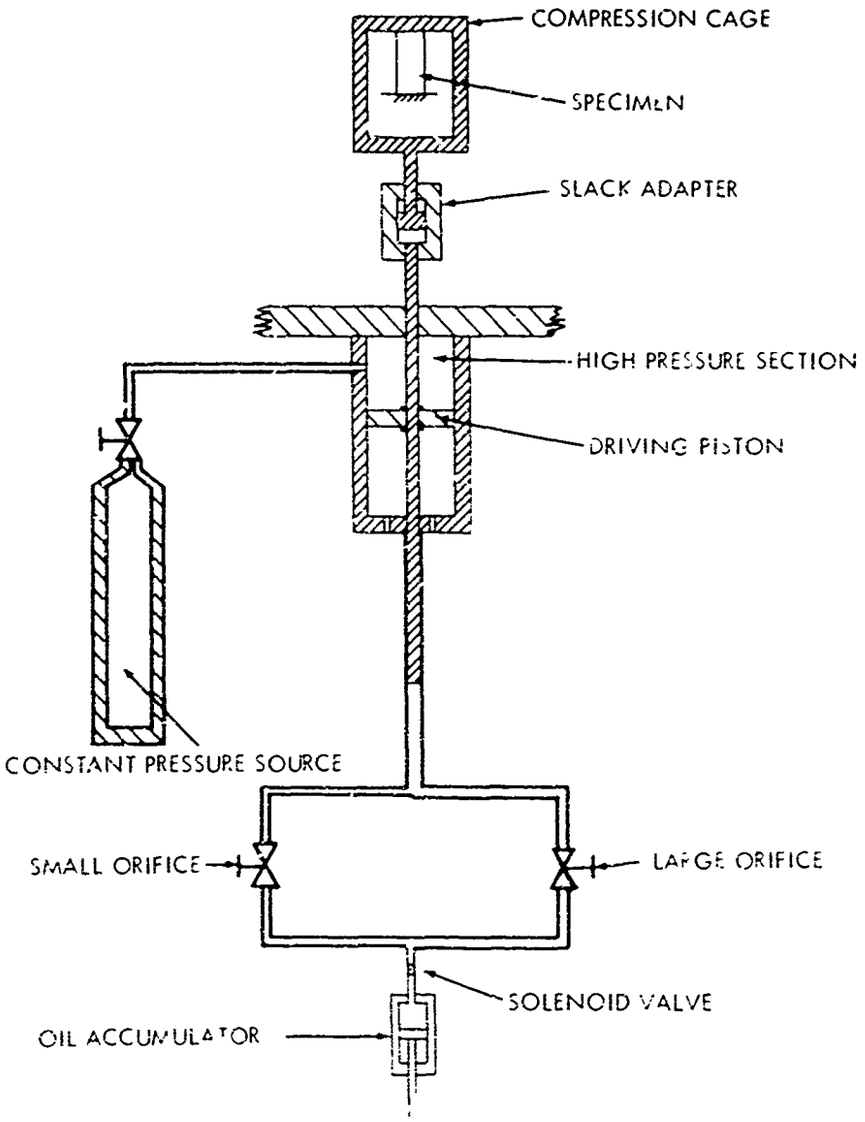

FIG. 14 SCHEMATIC DIAGRAM OF MEDIUM RATE APPARATUS

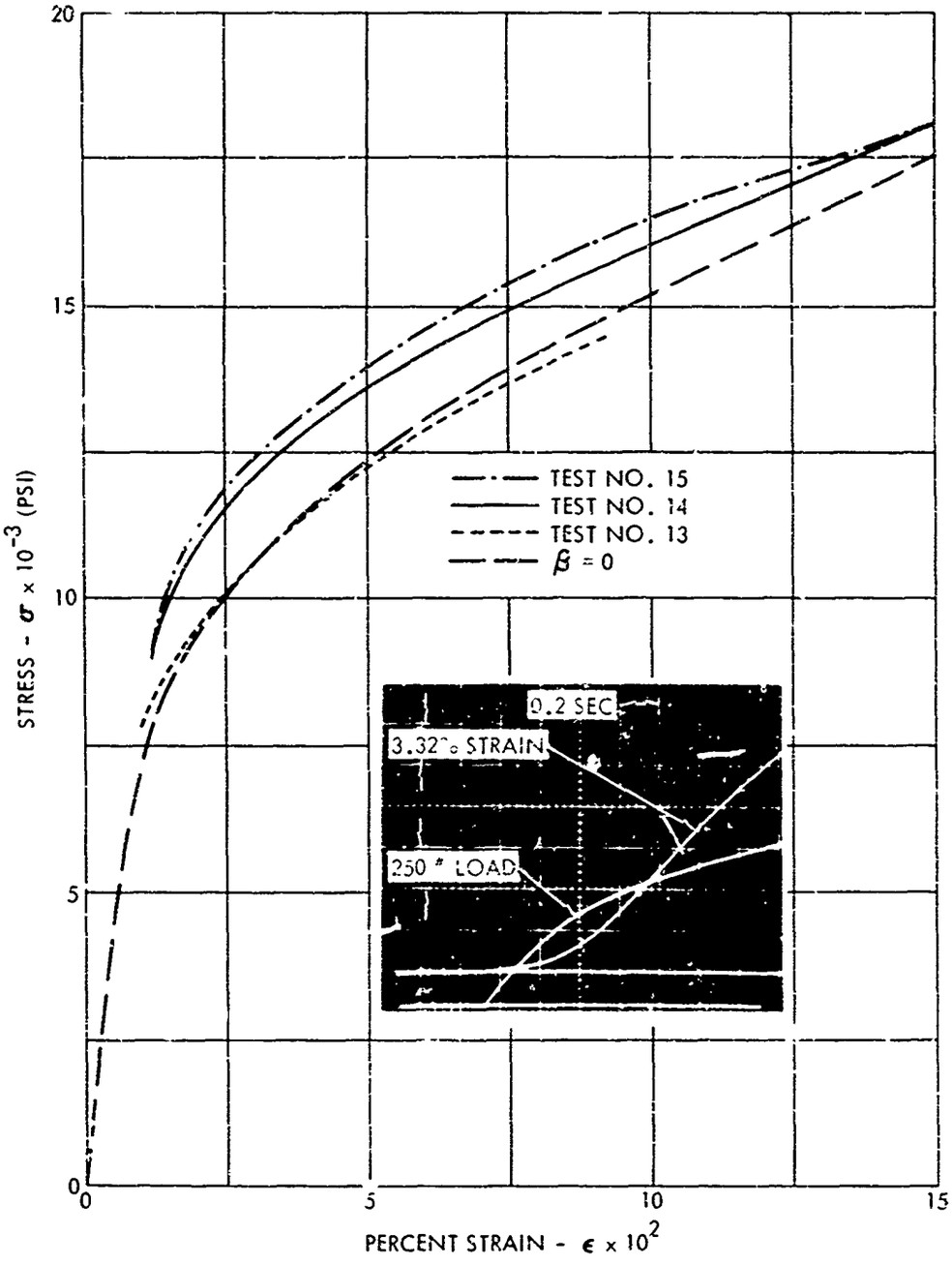

FIG. 15 STRESS-STRAIN BEHAVIOR OF ALUMINUM AT MEDIUM RATES

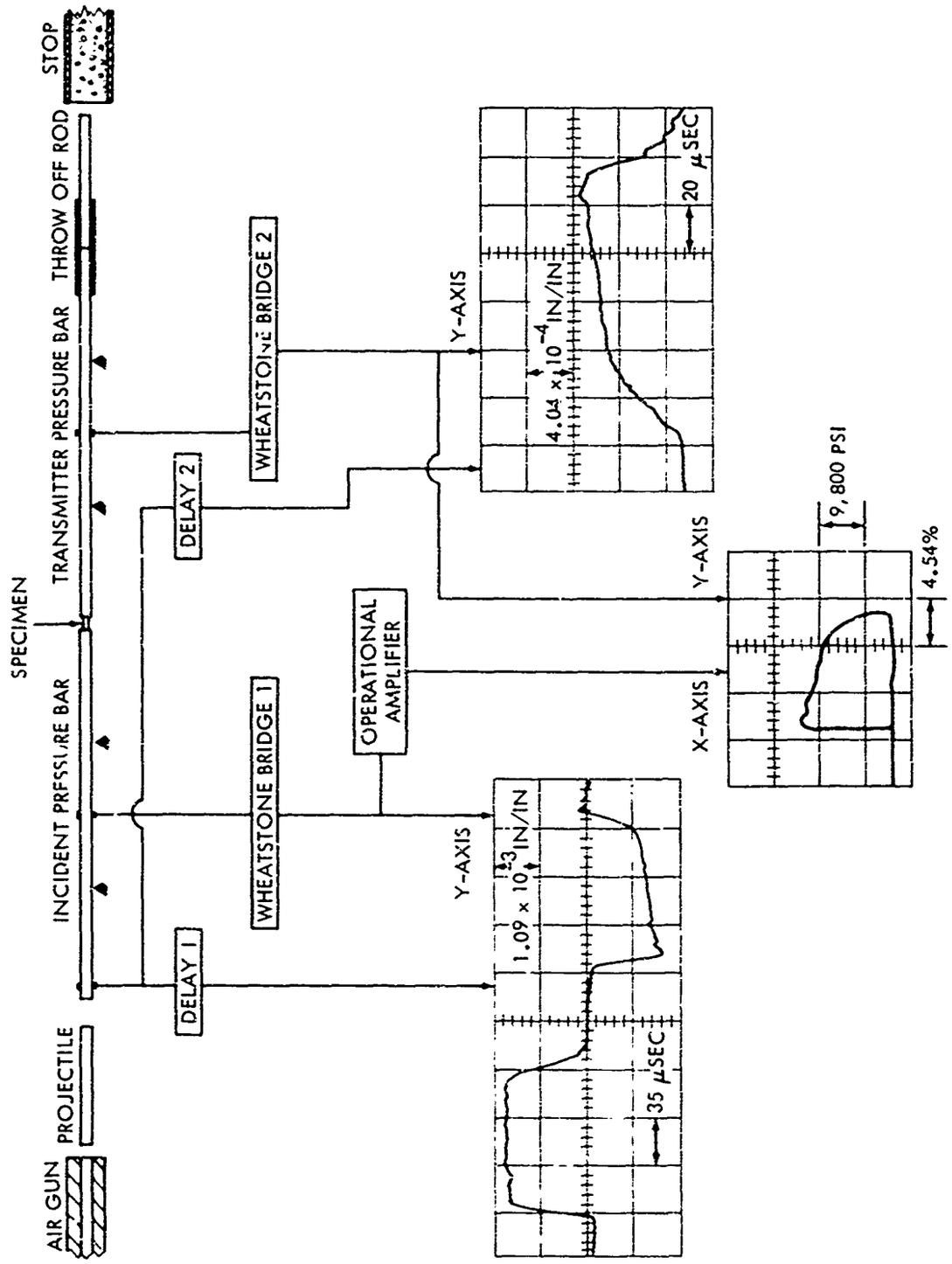

FIG. 16 SCHEMATIC REPRESENTATION OF SPLIT HOPKINSON PRESSURE BAR

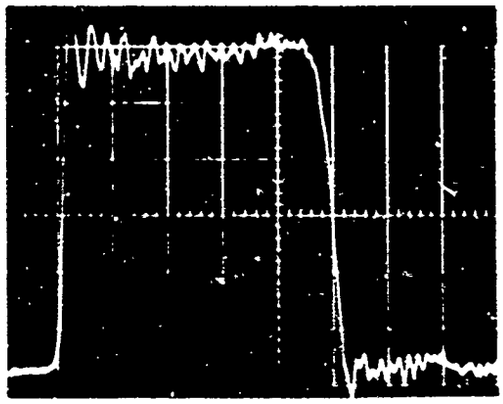

(A) IMPACT OF FLAT NOSED TITANIUM PROJECTILE ON TITANIUM PRESSURE BAR

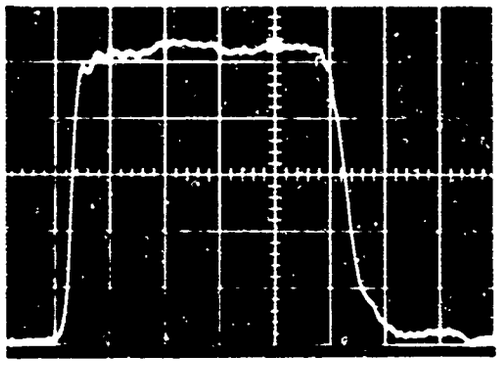

(B) IMPACT OF SPHERICAL NOSED (1" RADIUS) PROJECTILE ON TITANIUM PRESSURE BAR

FIG. 17 EFFECT OF PROJECTILE FACE ON INCIDENT PULSE

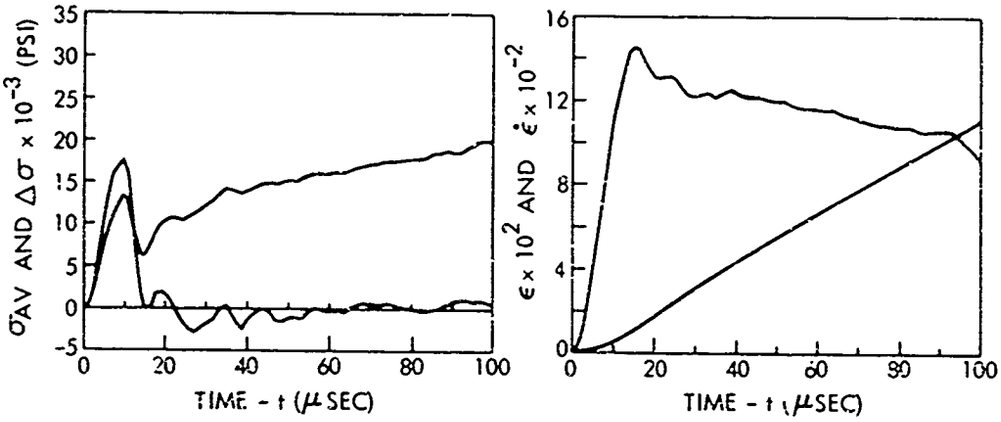

(A) STRESS AND STRESS DIFFERENCE OF SPECIMEN NO.19

(B) STRAIN AND STRAIN RATE OF SPECIMEN NO.19

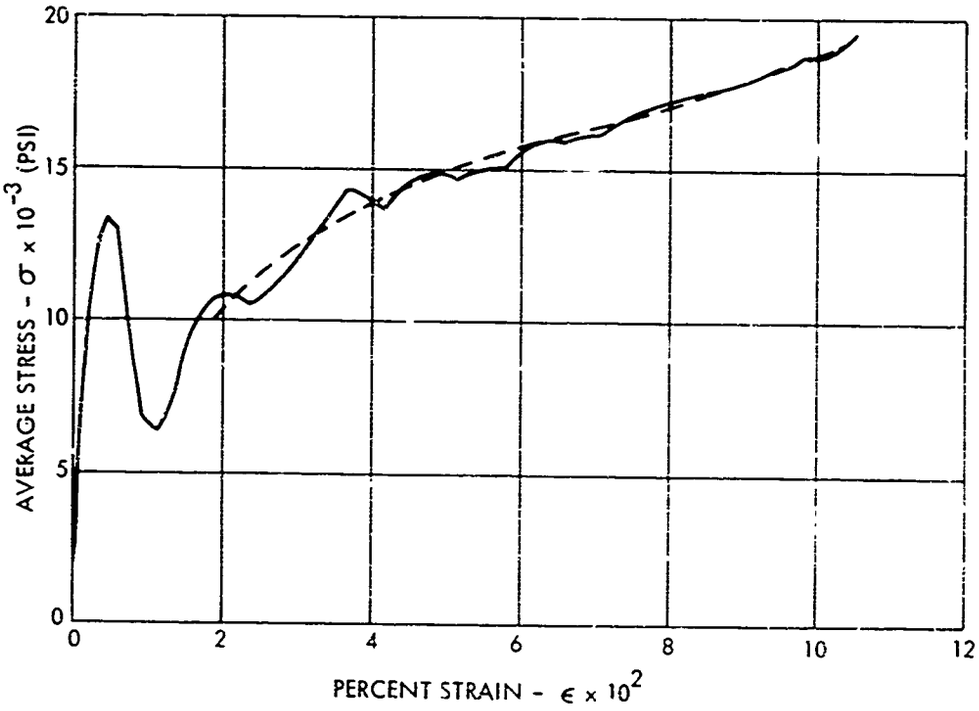

(C) STRESS-STRAIN BEHAVIOR OF SPECIMEN NO. 19

FIG. 18 TYPICAL DATA FOR COMMERCIALLY PURE ALUMINUM

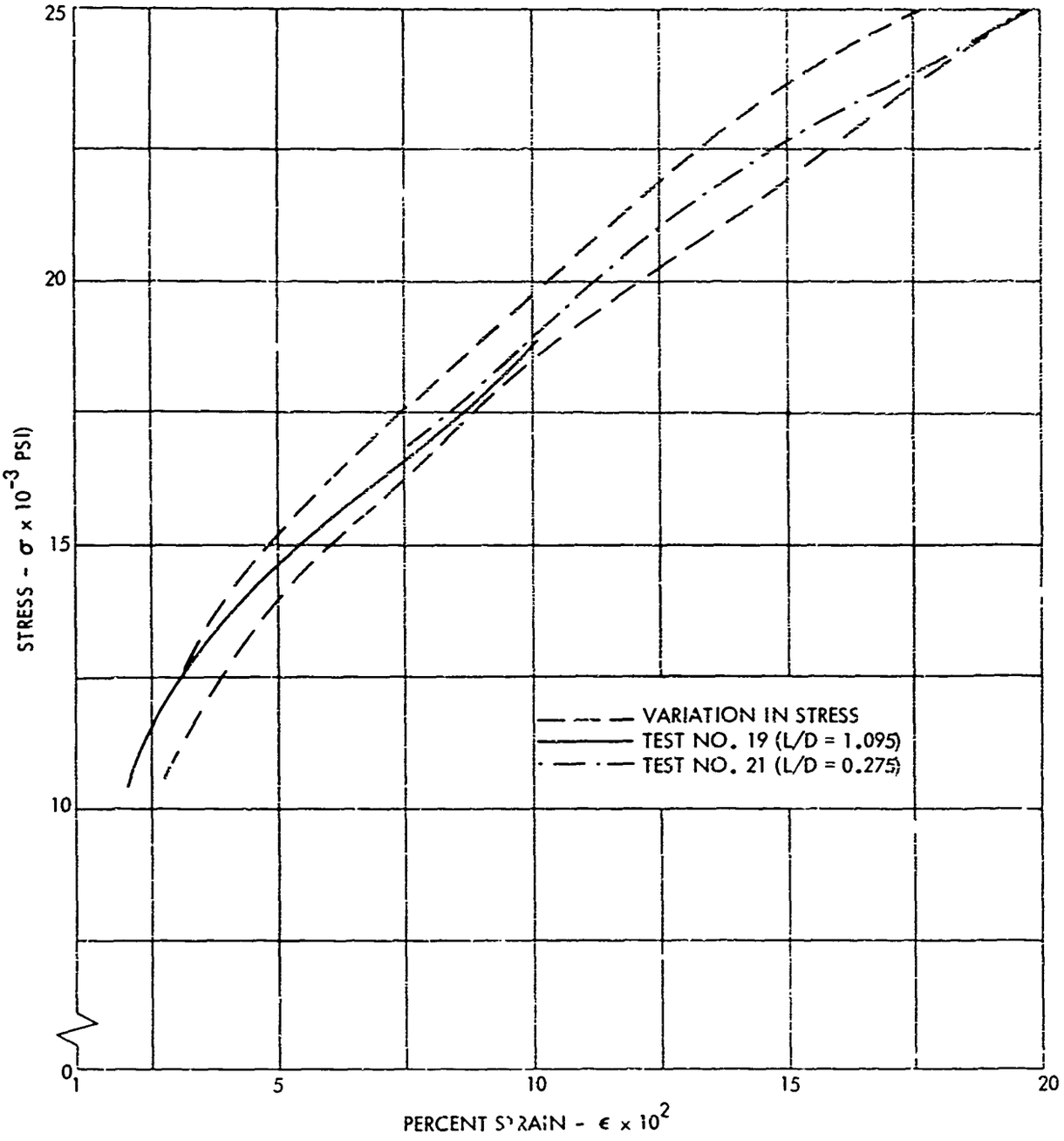

FIG. 19 EFFECT OF SPECIMEN GEOMETRY AND SPECTRUM OF STRESS-STRAIN BEHAVIOR AT HIGH STRAIN RATES

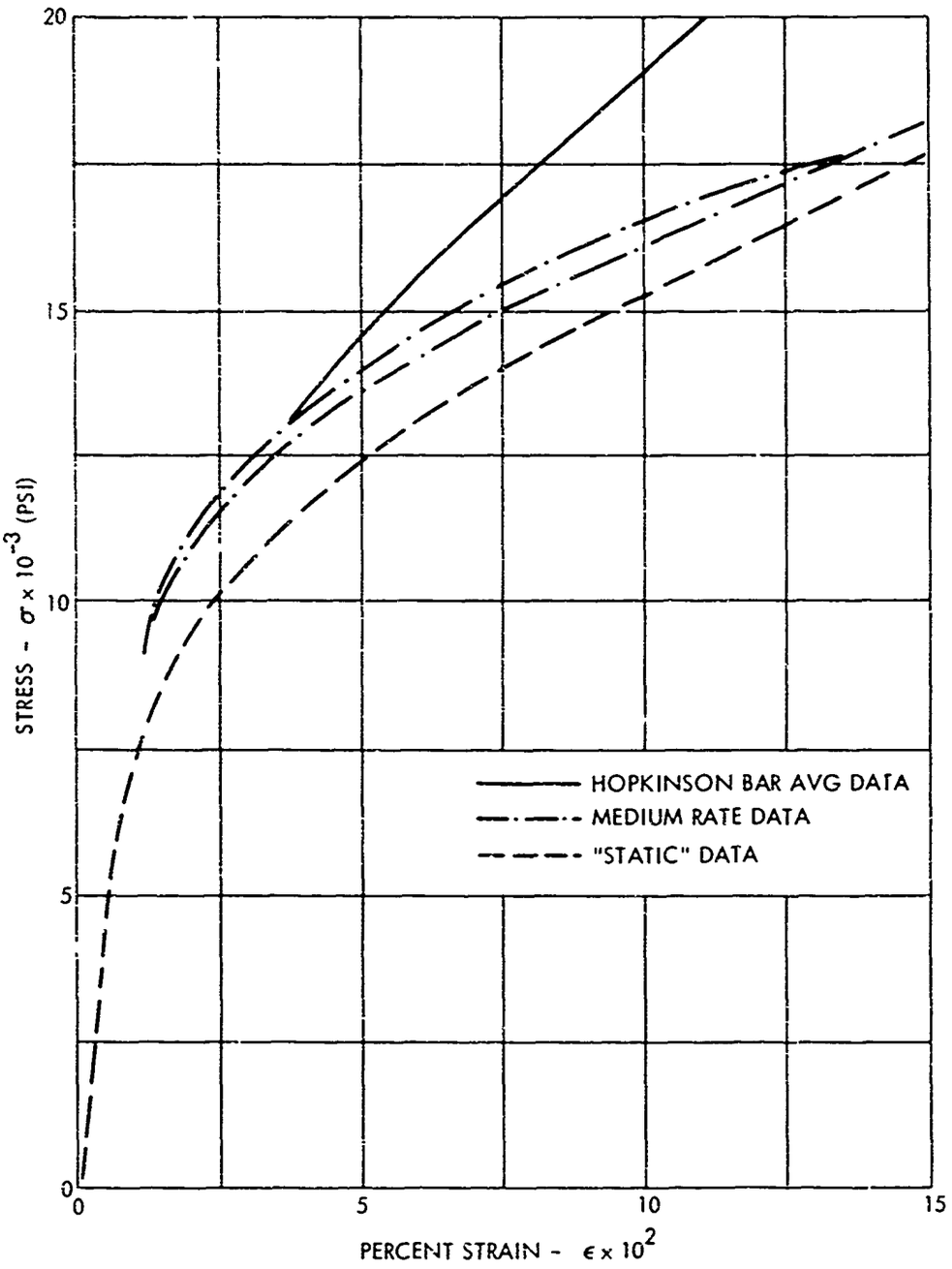

FIG. 20 VARIOUS OBSERVED BEHAVIOR OF COMMERCIALLY PURE ALUMINUM

APPENDIX A

THE ONE-DIMENSIONAL ANALYSIS

It is generally conceded that the one-dimensional theory of wave propagation will accurately predict the stresses, strains and particle velocities in long, thin rods where the area change is not large. However, in order to analyze the split Hopkinson pressure bar experiment, the equations must be applied not only to the pressure bars but to a specimen with an ℓ_o/d_o on the order of unity. Therefore, the response of the specimen must be calculated with the basic assumption that a uniaxial stress condition exists at all times. The validity of this assumption must ultimately be established experimentally.

The Pressure Bar

The one-dimensional analysis when applied to an elastic bar of constant original cross-sectional area requires that:

$$dv = \frac{d\sigma}{\rho_o c_o} \tag{A-1}$$

along lines in the a-t plane defined by:

$$\frac{da}{dt} = \pm c_o = \pm (E/\rho_o)^{\frac{1}{2}} \tag{A-2}$$

Therefore, along those lines of positive slope, integration of equation (A-1) yields:

$$v - \frac{\sigma}{\rho_o c_o} = K_p \tag{A-3}$$

Similarly, along those lines of negative slope:

$$v + \frac{\sigma}{\rho_o c_o} = K_n \tag{A-4}$$

The constants of integration K_p and K_n may be determined from the initial conditions, so that the problem is reduced to the simultaneous solution of two linear algebraic equations.

In order to demonstrate the application of these equations, consider the diagram in figure A-1. It is assumed that all components of the system are initially at rest and stress free. An arbitrary pulse has been generated at one end and has been

observed at the strain-measuring station located a distance x_I from the specimen. The constant K_p at the point I may be determined from the initial conditions and is equal to zero. From equation (A-3) it obviously follows that:

$$v_I = \frac{\sigma_I}{\rho_o c_o} = c_o \varepsilon_I \tag{A-5}$$

The value of K_n may be determined at point B from the values now known at point I. From equation (A-4) it is seen that:

$$v_B + \frac{\sigma_B}{\rho_o c_o} = v_I + \frac{\sigma_I}{\rho_o c_o} \tag{A-6}$$

However, from equation (A-5) we may substitute the value of v_I into equation (A-6) to yield:

$$v_B + \frac{\sigma_B}{\rho_o c_o} = 2c_o \varepsilon_I \tag{A-7}$$

In order to determine the value of K_n at point R, it is necessary to repeat the experiment in the absence of a specimen with the identical incident pulse shape, or otherwise generate the incident pulse so that the value of K_n may be determined in the absence of reflections from the specimen. For simplicity, let it be assumed that K_n may be determined at point D and is equal to zero. In this case,

$$v_R = - c_o \varepsilon_R \tag{A-8}$$

Applying equation (A-3) between points B and R yields:

$$v_B - \frac{\sigma_B}{\rho_o c_o} = v_R - \frac{\sigma_R}{\rho_o c_o} \tag{A-9}$$

Therefore,

$$v_B \frac{\sigma_B}{\rho_o c_o} = - 2c_o \varepsilon_R \tag{A-10}$$

Equations (A-7) and (A-10) may be solved simultaneously for the stress and particle velocity in terms of the measured quantities.

$$v_B = c_o(\varepsilon_I - \varepsilon_R) \tag{A-11}$$

and

$$\sigma_B = \rho_o c_o^2(\varepsilon_I + \varepsilon_R) = E(\varepsilon_I + \varepsilon_R) \qquad \text{(A-12)}$$

The initial conditions of the problem permit equation (A-3) to be applied between points F and C and between points E and T. Therefore:

$$v_C - \frac{\sigma_C}{\rho_o c_o} = v_F - \frac{\sigma_F}{\rho_o c_o} = 0 \qquad \text{(A-13)}$$

and

$$v_T - \frac{\sigma_T}{\rho_o c_o} = v_E - \frac{\sigma_E}{\rho_o c_o} = 0 \qquad \text{(A-14)}$$

Applying equation (A-4) between points C and T then yields:

$$v_C = c_o \varepsilon_T \qquad \text{(A-15)}$$

and

$$\sigma_C = \rho_o c_o^2 \varepsilon_T = E\varepsilon_T \qquad \text{(A-16)}$$

If the transmitted strain, ε_T, is measured at a distance x_T from the specimen, then the stress and particle velocity of the pressure bar at the specimen at time t_C will be determined from the transmitted strain record at time $(t_C + \frac{x_T}{c_o})$. Similarly, the pertinent incident and reflected strain data occur at $(t_B - \frac{x_I}{c_o})$ and $(t_B + \frac{x_I}{c_o})$, respectively. Knowledge of the stresses and particle velocities at each instant of time then permits the stress and strain in the specimen to be computed according to the definitions contained in reference 8.

The Specimen

Application of the one-dimensional theory of wave propagation to the specimen is somewhat more complicated since the paths along which the differential equations must be applied are no longer straight lines. In general, the differential equations may not be integrated in closed form and the many wave reflections

between the faces of the pressure bars must be taken into account. The solution to this problem may be carried out graphically and the details of this calculation are available in the literature [9]. Therefore, only the approach to this problem will be outlined here.

The stress and particle velocity at an arbitrary point in the specimen are determined by the simultaneous solution of the two differential equations which apply along the two lines that intersect at the arbitrary point in the a-t plane. As before:

$$dv = \frac{d\sigma}{\rho_o c} \tag{A-17}$$

however, the paths are now defined by the expression:

$$\rho_o c^2 \frac{\partial \epsilon}{\partial t} = \frac{\partial \sigma}{\partial t} \tag{A-18}$$

For a rate insensitive material or for a constant strain rate test, this expression may be simplified to yield the relation:

$$\rho_o c^2 = \left(\frac{\partial \sigma}{\partial \epsilon}\right)_{\dot{\epsilon}} \tag{A-19}$$

Therefore, along the positively sloped paths, integration of equation (A-17) yields:

$$v - v_1 = \varphi - \varphi_1 \tag{A-20}$$

where

$$d\varphi \equiv \left[\rho_o \left(\frac{\partial \sigma}{\partial \epsilon}\right)_{\dot{\epsilon}}\right]^{-\frac{1}{2}} d\sigma \tag{A-21}$$

Similarly, along the negatively sloped paths, integration yields:

$$v - v_2 = \varphi_2 - \varphi \tag{A-22}$$

At the boundary, between the incident pressure bar and the specimen, the magnitude of the incident stress wave in addition to the waves in the specimen will influence the motion of the interface. At any point on this boundary the characteristic paths to be considered are a positively sloped line in the specimen and a negatively sloped line in the pressure bar. In the first case we have from equation (A-20):

$$v_S - \varphi_S = v_1 - \varphi_1 \tag{A-23}$$

while in the second case:

$$v_B + \frac{\sigma_B}{\rho_o c_o} = 2c_o\varepsilon_I \tag{(A-7)}$$

The boundary conditions described in reference 8 may be expressed as follows:

$$v_S = v_B \tag{A-24}$$

and

$$\sigma_S A_S = \sigma_B A_B \tag{A-25}$$

The simultaneous solution of equations (A-7), (A-23), (A-24) and (A-25) yields the following expression from which the specimen stress may be determined:

$$\frac{\sigma_S A_S}{\rho_o c_o A_o} + \varphi(\sigma_S) = 2c_o\varepsilon_I - v_1 + \varphi_1 \tag{A-26}$$

Once the specimen stress is determined, the velocity may be obtained from equation (A-23). A similar treatment may be applied to the specimen-transmitter bar interface which results in the following expression:

$$\frac{\sigma_S A_S}{\rho_o c_o A_o} + \varphi(\sigma_S) = v_2 + \varphi_2 \tag{A-27}$$

which may be solved for the specimen stress. This stress then may be used to determine the velocity of the interface from the expression:

$$v_S = v_2 + \varphi_2 - \varphi(\sigma_S) \tag{A-28}$$

Providing the stress-strain relation for the specimen and the elastic constants of the pressure bars are known in advance, the stress, strain and velocity may be calculated at any point in the a-t plane, including the boundaries. Therefore, knowledge of the incident strain pulse permits the computation of both the

reflected and transmitted strain pulses. These results then may be used to compute the "apparent" stress-strain relation which will include the effects of nonlinear wave propagation in the specimen.

The CASH Code

Although the computation of the stresses and velocities in the specimen as a function of time and position is straightforward, the graphical method used by Conn [9] is extremely laborious if any degree of accuracy is desired. Therefore, this problem has been programmed in FORTRAN IV so that the task of evaluating the effects of axial wave propagation in this experiment may be lightened somewhat.

The CASH Code (an acronym for Characteristics Applied to the Split Hopkinson Bar) essentially divides the a-t plane into a number of lines of constant a. The point in time along each of these lines where the equations are to be evaluated is determined, as shown in figure A-2, by the preceding points on adjacent lines. The characteristic lines at the adjacent points are extended assuming no change in slope. In general, each line will intersect the desired line at a different time. The earliest arrival establishes the location of the point and the other line is shifted back in time until it intersects the same point. Shifting of the adjacent point is accomplished by a linear interpolation of the function, Φ, defined by equation (A-21). As this function changes, the slope of the characteristic line also changes until the resulting line intersects the desired point. The particle velocity then is linearly interpolated to the same point and all other required properties then are evaluated.

This program has been written utilizing several subroutines so that other problems in one-dimensional wave propagation may be solved without re-programming. The main routine is used to control the input of data, conversion to non-dimensional quantities and incrementing through the characteristic net. Since all of the equations used in the program have been non-dimensionalized with respect to the specimen yield stress, any consistent set of units may be used for input data. The shape of the incident strain pulse may be described by as many as 200 pairs (ϵ,t) of points which are constant or increasing in magnitude since the present subroutines have not been written to accommodate elastic unloading. Due to the number of points required to describe the details of the wave phenomenon, only ten points along each line of constant a are retained at any time. After the tenth point is computed, all ten points along lines for which output is desired then are stored and the next ten points may be computed.

Subroutine STORE is used to control the form of the output of data. This output may either be non-dimensional or have the same dimensions as the input data at the option of the user. After all quantities have been stored at 50 points along as many

as eleven lines of constant a, the results for each line then are printed separately.

Subroutine BOUND solves the characteristic equations at the boundaries of the specimen. Equation (A-26) which must be solved at the specimen-incident bar interface may be written as:

$$\left(\frac{\bar{\rho}_I \bar{A}_I}{\bar{C}_I}\right) S + P = 2\bar{C}_I \bar{E}_I - U_1 + P_1 \qquad \text{(A-26)}$$

where the non-dimensional quantities are defined in the list of symbols. Similarly, equation (A-27) which must be solved at the specimen-transmitter bar interface may be written as:

$$\left(\frac{\bar{\rho}_T \bar{A}_T}{\bar{C}_T}\right) S + P = U_2 + P_2 \qquad \text{(A-27)}$$

Therefore, both equations (A-26) and (A-27) are of the same form:

$$K_1 S + P = K_2 \qquad \text{(A-29)}$$

where K_1 and K_2 are constants which must be determined at each interface. Subroutine BOUND computes the value of each of these constants at each time and then uses a portion of subroutine WAVE, which contains the stress-strain relation of the specimen, to solve equation (A-29).

Subroutine STRESS solves the characteristic equations at all interior points in the a-t plane. It first establishes the point in time at which the equations are to be solved and controls the shifting of the characteristic line on one side. The equations to be solved take the form:

$$U - P = U_1 - P_1 \qquad \text{(A-20)}$$

and

$$U + P = U_2 + P_2 \qquad \text{(A-22)}$$

This subroutine uses another portion of subroutine WAVE in order to accomplish the shifting and establish the new characteristic quantities which are required to solve equations (A-20) and (A-22).

Subroutine WAVE is the only portion of this program which requires use of the stress-strain relation of the material. The

subroutine reported here is based on a stress-strain relation which has the form:

$$\bar{E} = S \qquad \text{for } S < 1 \qquad \text{(A-30)}$$

and

$$\bar{E} = B_1 + B_2 S + B_3 S^2 \qquad \text{for } S > 1 \qquad \text{(A-31)}$$

This equation was used since many materials may be represented with a stress-strain relation of this general shape [26] and all derivatives and integrals are easily obtained in closed form. The relationship between P and S becomes:

$$S = \frac{[3B_3(P - 1) + (B_2 + 2B_3)^{1.5}]^{\frac{2}{3}} - B_2}{2B_3} \qquad \text{(A-32)}$$

and

$$P = 1 + \frac{(B_2 + 2B_3 S)^{1.5} - (B_2 + 2B_3)^{1.5}}{3B_3} \qquad \text{(A-33)}$$

The slopes of the characteristics are given by:

$$\bar{C} = \pm (B_2 + 2B_3 S)^{-\frac{1}{2}} \qquad \text{(A-34)}$$

Therefore, the first portion of this subroutine is used to evaluate the stress, strain and characteristic slope for any given value of P. The second portion of this subroutine is used by subroutine BOUND. When equation (A-33) is substituted into equation (A-29), a cubic equation in S results which may be solved for its one real root. The third portion of subroutine WAVE is used to shift the required characteristics determined by subroutine STRESS. The method by which this shift is accomplished may be demonstrated by considering figure A-2. Subroutine STRESS is used to determine the point $T_{L,N}$ and identifies the point $T_{L-1,N}$ which needs to be shifted until:

$$T_{L-1,N} = T_{L,N} - (\bar{C}_{L-1,N})^{-1} \Delta a \qquad \text{(A-35)}$$

The slope of the required characteristic, $\bar{C}$, is determined by substitution of equation (A-34) into equation (A-33) and assuming that P varies linearly between $T_{L-1,N-1}$ and $T_{L-1,N}$. This results in a single equation for the unknown time, $T_{L-1,N}$, which may then

be evaluated. This time then is used to compute the values of P and V assuming a linear variation between $T_{L-1,N-1}$ and the former $T_{L-1,N}$. The stress, strain and characteristic slope then may be computed from equations (A-32), (A-33) and (A-34).

The solution of equation (A-29) and the shifting of characteristic quantities requires the solution of a standard cubic equation with one real root. Since this must be accomplished at almost every point in the characteristic net, a function subroutine has been included which evaluates the one root without the use of time-consuming iterative techniques.

The CASH Code provides a very rapid method for computing the one-dimensional response of the split Hopkinson pressure bar since there are no iterative schemes employed in the program. It is difficult to estimate the accuracy of this program because of the linear interpolations used throughout; however, as the number of points in the characteristic net is increased, the exact solution should be approached. The sample problem described in this report was computed with LMAX equal to 201 and again with LMAX equal to 51 with no apparent degradation of results. Since the computer time required is roughly proportional to the square of LMAX, the lower value is recommended for reasons of economy. The solution to the sample problem was carried out to a dimensionless time of 60 with LMAX equal to 51 and required 4.23 minutes on the IBM 7090 Version 13. A listing of the FORTRAN statements which constitute the CASH Code is provided in Appendix B.

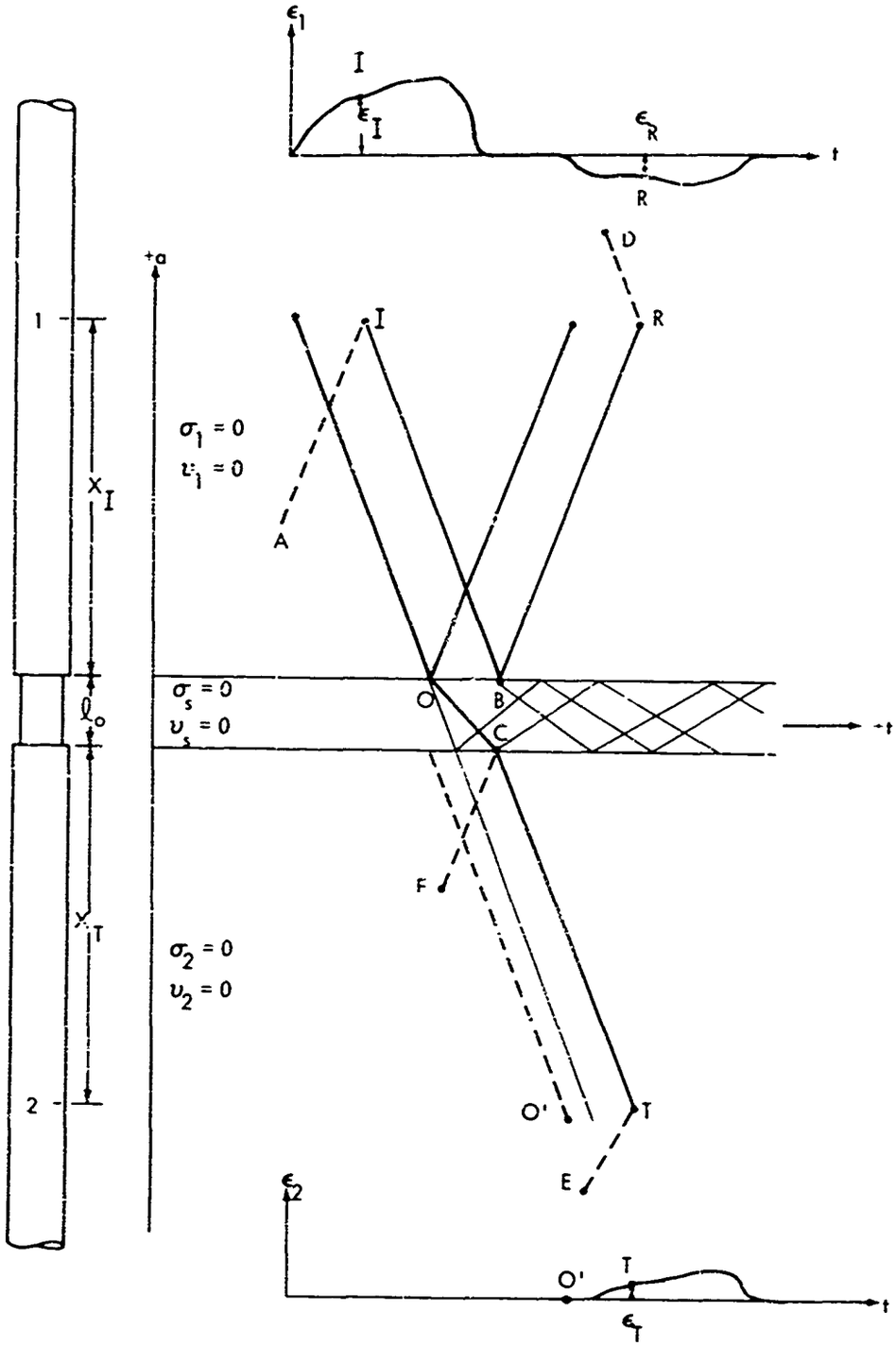

FIG. A-1 CHARACTERISTIC DIAGRAM OF EXPERIMENT

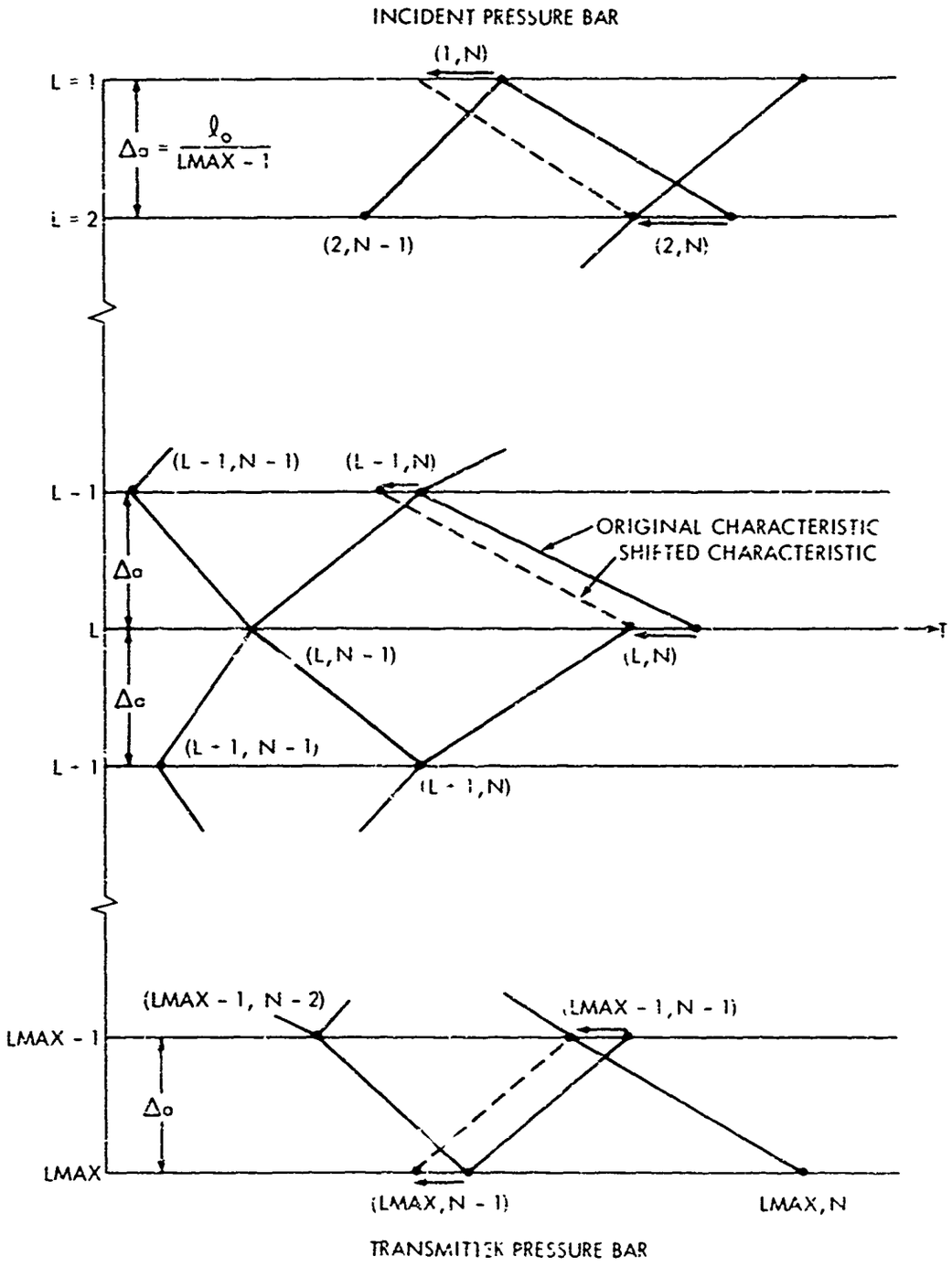

FIG. A-2 CHARACTERISTIC NET USED BY CASH CODE

THE CASH CODE

```
IbFTC CASH    LIST
      THIS PROGRAM COMPUTES THE TRANSIENT RESPONSE OF THE SPLIT
      HOPKINSON PRESSURE BAR EXPERIMENT BY THE METHOD OF CHARACTER-
      ISTICS ASSUMING THE RADIAL STRESS IS EQUAL TO ZERO.  THE MAIN
      ROUTINE, CASH, FORMS ALL VARIABLES INTO NON-DIMENSIONAL QUANTI-
      TIES, ESTABLISHES THE ZONING, AND CONTROLS THE INDEXING THROUGH
      THE CHARACTERISTICS NET.  THE FOLLOWING DICTIONARY OF TERMS MAY
      PROVE HELPFUL IN MAKING CHANGES TO THIS PROGRAM.

      PROGRAM SYMBOL                DEFINITION
            S           STRESS/SPECIMEN YIELD STRESS
            U           PARTICLE VELOCITY/IMPACT VELOCITY AT YIELD
            E           STRAIN/SPECIMEN YIELD STRAIN
            C           WAVE VELOCITY/ELASTIC WAVE VELOCITY
            P           IMPACT VELOCITY/IMPACT VELOCITY AT YIELD
            T           TIME/TIME FOR ELASTIC WAVE TO TRAVERSE SPECIMEN

      THE FOLLOWING INSTRUCTIONS ARE TO ASSIST THE USER IN PREPARING
      THE DATA DECK.  ANY CONSISTENT SET OF UNITS MAY BE USED...
      (I.E. IN, PSI, IN/SEC, ETC.)

            COL
      CARD 1 1-14 D1          INCIDENT BAR DIAMETER
            15-28 E1          INCIDENT BAR MODULUS
            29-42 RHO1        INCIDENT BAR DENSITY

      CARD 2 1-14 D2          TRANSMITTER BAR DIAMETER
            15-28 E2          TRANSMITTER BAR MODULUS
            29-42 RHO2        TRANSMITTER BAR DENSITY

      CARD 3 1-14 DS          SPECIMEN DIAMETER
            15-28 ES          SPECIMEN MODULUS
            29-42 RHOS        SPECIMEN DENSITY
            43-56 SY          SPECIMEN YIELD STRESS (MUST BE NON-ZERO)

      CARD 4 1-14 G           DIMENSIONAL CONVERSION FACTOR (386.086 IN/
                              SEC**2, OR 1.00 CM/SEC**2)
            15-28 XO          ORIGINAL SPECIMEN LENGTH

      CARD 5 1-14 B1          ARBITRARY CONSTANTS WHICH DESCRIBE THE
            15-28 B2          STRESS-STRAIN RELATION OF THE SPECIMEN
            29-42 B3          IN NON-DIMENSIONAL UNITS (SEE SUBROUTINE
            43-56 B4          WAVE).
            57-70 B5

      CARD 6 1-72 ID          ANY 72 CHARACTERS WILL BE PRINTED FOR
                              IDENTIFICATION PURPOSES

      CARD 7 4-5  I           ANY INTEGER FROM 2 TO 11 WHICH INDICATES
                              THE NUMBER OF POSITIONS ALONG THE SPECIMEN
                              THAT OUTPUT IS DESIRED
             8-10 LMAX        ANY ODD INTEGER FROM 3 TO 201 WHICH
                              DICTATES THE SIZE OF THE CHARACTERISTIC NET
               15 M           ENTER 1 IN COL 15 IF OUTPUT IS TO BE
                              DIMENSIONLESS.  LEAVE BLANK IF OUTPUT IS
                              DESIRED IN SAME UNITS AS INPUT.

      CARD 8 1-5  K           THE ACTUAL NUMBER OF PAIRS OF DATA POINTS
                              TO BE READ IN (MAY NOT EXCEED 200)
             6-19 C1          A CONSTANT WHICH WILL CONVERT THE INPUT
```

APPENDIX B

	20-33 C2	DATA TO UNITS OF STRAIN A CONSTANT WHICH WILL CONVERT THE INPUT DATA TO UNITS OF TIME
CARD 913-18	EPS1(J)	4 PAIRS OF DATA POINTS PER CARD WHICH ARE
	19-24 TIM(J)	PROPORTIONAL TO THE STRAIN AND TIME OF THE INCIDENT PULSE
CARD 101-5	KKK	CONTROL CARD WHICH DICTATES THE RETURN FOR SUBSEQUENT CASES... -1 = RETURN TO CARD 1 0 = RETURN TO CARD 3 +1 = RETURN TO CARD 8

```
      COMMON A,A1,A2,A3,A4,A5,AREA1,AREA2,B,B1,B2,B3,B4,B5,BE,C(201,12),
     1C1,C2,CBAR1,CBAR2,CE,CO(11,50),CR,CS,CW,D1,D2,DC,DS,DT,DX,E(201,12
     2),E1,E2,EF(12),EO(11,50),EPS1(200),EPS2(12),ER,ERO(50),ES,ET(12),
     3ETO(50),EW,G,I,II,ID(12),J,K,L,LL,LLL(11),LMAX,LMAX1,LMAX2,M,N,NN,
     4NMAX,NPAGE,NSTORE,P(201,12),P1,P2,PO(11,50),PP,PR,PW,RHO1,RHO2,
     5RHOS,S(201,12),SLOPE,SMAX(201),SO(11,50),SR,SS,SW,SY,T(201,12),T1,
     6T2,TIM(200),TO(11,50),TR,TS,U(201,12),UO(11,50),UR,US,XBAR(11),XO
  200 READ (5,1) D1,E1,RHO1
      READ (5,1) D2,E2,RHO2
  205 READ (5,1) DS,ES,RHOS,SY
      READ (5,1) G,XO
      READ (5,1) B1,B2,B3,B4,B5
      READ (5,5) ID
      READ (5,2) I, LMAX,M
  210 READ (5,3) K,C1,C2
      READ (5,4) (EPS1(J),TIM(J), J=1,K)
      WRITE (6,6) ID
      WRITE (6,7)   D1,E1,RHO1,D2,E2,RHO2,DS,ES,RHOS,SY
      WRITE (6,8) B1,B2,B3,B4,B5
      WRITE (6,9) I,LMAX,K
      NSTORE = 0
      NPAGE = 0
      DO 10 L=1,LMAX
      U(L,1)=0.
      S(L,1)=0.
      C(L,1)=1.
      E(L,1)=0.
      T(L,1)=0.
      P(L,1)=0.
      SMAX(L)=1.
   10 CONTINUE
      EF(1)=0.
      ET(1)=0.
      EPS2(1)=0.
      AREA1=(DS/D1)**2.
      AREA2=(DS/D2)**2.
      CBAR1=SQRT(E1*RHOS/(ES*RHO1))
      CBAR2=SQRT(E2*RHOS/(ES*RHO2))
      CS=SQRT(ES*G/RHOS)
      A1=SY/ES
      A2=CS*A1
      A3=XO/CS
      A4=1.+RHOS*AREA1/(RHO1*CBAR1)
      A5=1.+RHOS*AREA2/(RHO2*CBAR2)
      C2=C2/A3
      LMAX1 = LMAX - 1
```

APPENDIX B

```
      A = LMAX1
      LMAX2=LMAX1-1
      DX=1./A
      XBAR(1)=0.
      I1=I-1
      DO 20 J=1,I1
      B=FLOAT(J)/FLOAT(I1)
      XBAR(J+1)=B
   20 CONTINUE
      DO 350 II=1,I
      LLL(II) = XBAR(II) * FLOAT(LMAX1) + 1.
  350 CONTINUE
      J=2
      SLOPE=C1*FPS1(2)/(C2*TIM(2))
      T(1,2)=2.*DX
      EPS2(2)=SLOPE*DX*2.
      DO 60 L=2,LMAX1,2
      T(L,1)=DX
   60 CONTINUE
      L=1
      N=2
      S(1,2) = (2.*CBAR1*EPS2(2)*ES)/(SY*(1.+ALFA1*RHOS/(CBAR1*RHO1)))
      P(1,2)=S(1,2)
      C(1,2) =1.
      E(1,2) = S(1,2)
      U(1,2)=P(1,2)
      IF (S(1,2)-1.) 64,64,62
   62 SMAX(1)=S(1,2)
   64 DO 70 L=3,LMAX,2
      P(L,2)=0.
      S(L,2)=0.
      U(L,2)=0.
      E(L,2)=0.
      C(L,2)=1.
      T(L,2)=2.*DX
   70 CONTINUE
      DO 80 L=2,LMAX1,2
      P(L,2)=0.
      S(L,2)=0.
      U(L,2)=0.
      E(L,2)=0.
      C(L,2)=1.
      T(L,2)=3.*DX
   80 CONTINUE
      P(2,2)=P(1,2)
      S(2,2)=S(1,2)
      U(2,2)=U(1,2)
      E(2,2)=E(1,2)
   81 DO 110 N=3,12
      N=N
      L=1
      CALL BOUND
      DO 90 L=3,LMAX2,2
      L=L
      NN=N-1
      CALL STRESS
   90 CONTINUE
   91 DO 95 L=2,LMAX1,2
      IF (S(L,N-1) - SMAX(L))  95,95,92
   92 SMAX(L) = S(L,N-1)
```

```
 95 CONTINUE
    L=LMAX
    CALL BOUND
    DO 100 L=2,LMAX1,2
    L=L
    NN=N
    CALL STRESS
100 CONTINUE
101 DO 105 L=1,LMAX,2
    IF (S(L,N)-SMAX(L)) 105,105,102
102 SMAX(L)=S(L,N)
105 CONTINUE
    IF (T(1,N) .LT. 0.)  GO TO 990
    IF (S(1,N) .LT. 0.)  GO TO 980
    IF (S(LMAX,N) .LT. 0.) GO TO 985
    IF (J-K) 110,110,990
110 CONTINUE
    CALL STORE
130 DO 140 L=1,LMAX
    T(L,1)=T(L,11)
    S(L,1)=S(L,11)
    U(L,1)=U(L,11)
    E(L,1)=E(L,11)
    C(L,1)=C(L,11)
    P(L,1)=P(L,11)
    P(L,2)=P(L,12)
    T(L,2)=T(L,12)
    S(L,2)=S(L,12)
    U(L,2)=U(L,12)
    E(L,2)=E(L,12)
    C(L,2)=C(L,12)
140 CONTINUE
    EPS2(1)=EPS2(11)
    EPS2(2)=EPS2(12)
    EF(1)=EF(11)
    EF(2)=EF(12)
    ET(1)=ET(11)
    ET(2)=ET(12)
    GO TO 81
980 CALL STORE
    CALL OUTPUT
    WRITE (6,981)
    GO TO 150
985 CALL STORE
    CALL OUTPUT
    WRITE (6,986)
    GO TO 150
990 CALL STORE
    CALL OUTPUT
    GO TO 150
  1 FORMAT (5E14.5)
  2 FORMAT (3I5)
  3 FORMAT (I5,2E14.5)
  4 FORMAT (12X,8F6.0)
  5 FORMAT (12A6)
  6 FORMAT (1H1,12A6)
  7 FORMAT (1H-,24X,8HDIAMETER,12X,7HMODULUS,13X,7HDENSITY,11X,12HYIEL
   1D STRESS/13H0INCIDENT BAR,3X,3E20.8/16HOTRANSMITTER BAR,3E20.8/
   29HOSPECIMEN,7X,4E20.8)
  8 FORMAT (1H-,12X,2HB1,18X,2HB2,18X,2HB3,18X,2HB4,18X,2HB5/5E20.8)
  9 FORMAT (1H-,3HI =,I5,20X,6HLMAX =,I5,20X,3HK =,I5)
981 FORMAT (1H0,62HSPECIMEN HAS SEPERATED FROM INCIDENT BAR - ANALYSIS
   1 TERMINATED)
986 FORMAT (1H0,65HSPECIMEN HAS SEPERATED FROM TRANSMITTER BAR - ANALY
   1SIS TERMINATED)
150 CONTINUE
    READ (5,2) KKK
    IF (KKK) 200,205,210
999 STOP
    END
```

APPENDIX B

```
$IBFTC STORE   LIST
      SUBROUTINE STORE
       SUBROUTINE STORE CONVERTS THE NON-DIMENSIONAL QUANTITIES INTO THE
       SAME UNITS USED FOR INPUT.  THIS CONVERSION MAY BE SUPPRESSED BY
       ENTERING A 1 IN COL 15, CARD 7.  THE OUTPUT WILL THEN BE IN
       THE DIMENSIONLESS FORM INDICATED IN THE PROGRAM DICTIONARY.
       REFLECTED AND TRANSMITTED STRAIN VALUES ARE ALWAYS IN THE ACTUAL
       UNITS OF STRAIN (IN/IN).
      COMMON A,A1,A2,A3,A4,A5,AREA1,AREA2,B,B1,B2,B3,B4,B5,BF,C(201,12),
     1C1,C2,CBAR1,CBAR2,CF,CO(11,50),CR,CS,CW,D1,D2,DC,DS,DT,DX,E(201,12
     2),E1,E2,EF(12),EO(11,50),EPS1(200),EPS2(12),ER,ERO(50),ES,ET(12),
     3ETO(50),EW,G,I,II,ID(12),J,K,L,LL,LLL(11),LMAX,LMAX1,LMAX2,M,N,NN,
     4NMAX,NPAGE,NSTORE,P(201,12),P1,P2,PO(11,50),PP,PR,PW,RHO1,RHO2,
     5RHOS,S(201,12),SLOPE,SMAX(201),SO(11,50),SR,SS,SW,SY,T(201,12),T1,
     6T2,TIM(200),TO(11,50),TR,TS,U(201,12),UO(11,50),UP,US,XBAR(11),XO
       KK = N-2
       DO 905 N=1,KK
       NSTORE = NSTORE + 1
       DO 900 LOUT=1,I
       L = LLL(LOUT)
       IF (M .EQ. 1) GO TO 902
       TO(LOUT,NSTORE) = T(L,N) * A3
       SO(LOUT,NSTORE) = S(L,N) * SY
       PO(LOUT,NSTORE) = P(L,N) * A2
       UO(LOUT,NSTORE) = U(L,N) * A2
       EO(LOUT,NSTORE) = E(L,N) * A1
       CO(LOUT,NSTORE) = C(L,N) * CS
       GO TO 900
  902  TO(LOUT,NSTORE) = T(L,N)
       SO(LOUT,NSTORE) = S(L,N)
       PO(LOUT,NSTORE) = P(L,N)
       UO(LOUT,NSTORE) = U(L,N)
       EO(LOUT,NSTORE) = E(L,N)
       CO(LOUT,NSTORE) = C(L,N)
  900  CONTINUE
       ERO(NSTORE) = EF(N)
       ETO(NSTORE) = ET(N)
  905  CONTINUE
       IF (NSTORE .EQ. 50)  GO TO 901
       RETURN
       ENTRY OUTPUT
  901  NPAGE = NPAGE + 1
       DO 920 LOUT=1,I
       WRITE (6,910) XBAR(LOUT), NPAGE
       WRITE (6,911) (TO(LOUT,JJ),SO(LOUT,JJ),PO(LOUT,JJ),UO(LOUT,JJ),
      1 EO(LOUT,JJ),CO(LOUT,JJ), JJ=1,NSTORE)
  920  CONTINUE
       WRITE (6,930) NPAGE
       WRITE (6,931) (TO(1,JJ),ERO(JJ), JJ=1,NSTORE)
       LOUT = LLL(I)
       WRITE (6,940) NPAGE
       WRITE (6,931) (TO(I,JJ),ETO(JJ), JJ=1,NSTORE)
       NSTORE = 0
       RETURN
  910  FORMAT (1H1,6HXBAR =,F7.5,99X,4HPAGE,I4/1H0,11X,4HTIME,15X,6HSTRES
      1S,15X,3HPHI,10X,17HPARTICLE VELOCITY,9X,6HSTRAIN,12X,10HWAVE SPEED
      2)
  911  FORMAT (6E20.8)
  930  FORMAT (1H1,12HINCIDENT BAR,100X,4HPAGE,I4/1H0,11X,4HTIME,10X,
      1 16HREFLECTED STRAIN)
  931  FORMAT (2E20.8)
  940  FORMAT (1H1,15HTRANSMITTER BAR,97X,4HPAGE,I4/1H0,11X,4HTIME,9X,
      1 18HTRANSMITTED STRAIN)
       END
```

APPENDIX B

```
$IBFTC BOUND   LIST
      SUBROUTINE BOUND
       SUBROUTINE BOUND SOLVES THE CHARACTERISTIC EQUATIONS AT THE
       BOUNDARIES OF THE SPECIMEN.  THIS SUBROUTINE ASSUMES THAT THE
       SPECIMEN-PRESSURE BAR INTERFACE IS FRICTIONLESS AND THAT THE
       AXIAL FORCE AND VELOCITY OF THE SPECIMEN AND PRESSURE BAR ARE
       EQUAL.
      COMMON A,A1,A2,A3,A4,A5,AREA1,AREA2,B,B1,B2,B3,B4,B5,BE,C(201,12),
     1C1,C2,CBAR1,CBAR2,CE,CO(11,50),CR,CS,CW,D1,D2,DC,DS,DT,DX,E(201,12
     2),E1,E2,EF(12),EO(11,50),EPS1(200),EPS2(12),ER,ERO(50),ES,ET(12),
     3ETO(50),EW,G,I,II,ID(12),J,K,L,LL,LLL(11),LMAX,LMAX1,LMAX2,M,N,NN,
     4NMAX,NPAGE,NSTORE,P(201,12),P1,P2,PO(11,50),PP,PR,PW,RHO1,RHO2,
     5RHOS,S(201,12),SLOPE,SMAX(201),SO(11,50),SR,SS,SW,SY,T(201,12),T1,
     6T2,TIM(200),TO(11,50),TR,TS,U(201,12),UO(11,50),UR,US,XBAR(11),XO
       IF (L-1) 700,700,800
  700 T(1,N)=T(2,N-1) + DX/C(2,N-1)
       IF (T(1,N)-C2*TIM(J)) 704,704,702
  702 J=J+1
       SLOPE=C1*(EPS1(J)-EPS1(J-1))/(C2*(TIM(J)-TIM(J-1)))
  704 EPS2(N) = C1*EPS1(J-1)+SLOPE*(T(1,N)-C2*TIM(J-1))
  705 NN=N-1
       P1=RHOS*AREA1/(RHO1*CBAR1)
       P2=P(2,N-1)-U(2,N-1)+2.*CBAR1*EPS2(N)*ES/SY
       CALL PROP
       P(1,N)=PP
       PW=PP
       CALL WAVE
       S(1,N)=SW
       C(1,N)=CW
       E(1,N)=EW
       U(1,N)=2.*CBAR1*EPS2(N)*ES/SY-P1*SW
       EF(N)=0.5*(S(1,N)*AREA1*SY/E1-U(1,N)*SY/(CBAR1*ES))
       GO TO 850
  800 T(LMAX,N)=T(LMAX-1,N-1)+DX/C(LMAX-1,N-1)
       P1=RHOS*AREA2/(RHO2*CBAR2)
       P2=U(LMAX-1,N-1)+P(LMAX-1,N-1)
       CALL PROP
       PW=PP
       CALL WAVE
       P(LMAX,N)=PW
       S(LMAX,N)=SW
       C(LMAX,N)=CW
       E(LMAX,N)=EW
       U(LMAX,N)=P1*SW
       ET(N)=S(LMAX,N)*AREA2*SY/E2
  850 CONTINUE
       RETURN
       END
```

APPENDIX B

```
$IBFTC STRESS  LIST
      SUBROUTINE STRESS
       SUBROUTINE STRESS SOLVES THE CHARACTERISTIC EQUATIONS AT ALL
       INTERIOR POINTS OF THE SPECIMEN ASSUMING NO INITIAL CHANGE IN
       CROSS-SECTIONAL AREA.
      COMMON A,A1,A2,A3,A4,A5,AREA1,AREA2,B,B1,B2,B3,B4,B5,BE,C(201,12),
     1C1,C2,CBAR1,CBAR2,CE,CO(11,50),CR,CS,CW,D1,D2,DC,DS,DT,DX,E(201,12
     2),E1,E2,EE(12),EO(11,50),EPS1(200),EPS2(12),ER,ERO(50),ES,ET(12),
     3ETO(50),EW,G,I,I1,ID(12),J,K,L,LL,LLL(11),LMAX,LMAX1,LMAX2,M,N,NN,
     4NMAX,NPAGE,NSTORE,P(201,12),P1,P2,PO(11,50),PP,PR,PW,PHO1,RHO2,
     5RHOS,S(201,12),SLOPE,SMAX(201),SO(11,50),SP,SS,SW,SY,T(201,12),T1,
     6T2,TIM(200),TO(11,50),TP,TS,U(201,12),UO(11,50),UR,US,XBAR(11),XO
       T1=T(L-1,NN )+(DX/C(L-1,NN ))
       T2=T(L+1,NN )+(DX/C(L+1,NN ))
       IF (ABS(T1/T2 - 1.) .LE. 0.0000001)   GO TO 420
       IF (T1-T2) 400,420,410
  400 T(L,N)=T1
       LL=L+1
       CALL SHIFT
       GO TO 415
  410 T(L,N)=T2
       LL=L-1
       CALL SHIFT
       IF (L-2) 415,411,415
  411 IF (TR-C2*TIM(J-1)) 412,413,413
  412 J=J-1
       SLOPE = C1*(EPS1(J)-EPS1(J-1))/(C2*(TIM(J)-TIM(J-1)))
  413 EPS2(N)=C1*EPS1(J-1)+C1*(EPS1(J)-EPS1(J-1))*(TR-C2*TIM(J-1))/
      1 (C2*(TIM(J)-TIM(J-1)))
  415 P(LL,NN)=PP
       S(LL,NN)=SP
       E(LL,NN)=ER
       U(LL,NN)=UR
       C(LL,NN)=CR
       T(LL,NN)=TP
       GO TO 450
  420 T(L,N)=T1
  450 CONTINUE
       IF (L.EQ.1) GO TO 480
       P(L,N)=.5*(P(L+1,NN )+P(L-1,NN )-U(L+1,NN )+U(L-1,NN ))
       U(L,N)=.5*(U(L+1,NN )+U(L-1,NN )-P(L+1,NN )+P(L-1,NN ))
       IF (ABS(P(L,N)/P(L,N-1) - 1.) .LE. 0.0000001)   GO TO 479
       IF (P(L,N)-P(L,N-1)) 455,479,475
  455 S(L,N)=0.5*(S(L+1,NN)+S(L-1,NN)+U(L-1,NN)-U(L+1,NN))
       U(L,N)=0.5*(S(L-1,NN)-S(L+1,NN)+U(L-1,NN)+U(L+1,NN))
  470 P(L,N)=S(L,N)
       C(L,N)=1.
       E(L,N)=E(L,N-1)+S(L,N)-S(L,N-1)
       GO TO 480
  475 PW=P(L,N)
       CALL WAVE
       S(L,N)=SW
       C(L,N)=CW
       E(L,N)=EW
       RETURN
  479 S(L,N) = S(L,N-1)
       E(L,N) = E(L,N-1)
       C(L,N) = C(L,N-1)
  480 CONTINUE
       RETURN
       END
```

APPENDIX B

```
$IBFTC WAVE1   LIST
      SUBROUTINE WAVE
       SUBROUTINE WAVE IS THE ONLY SUBROUTINE WHICH REQUIRES USE OF THE
       STRESS-STRAIN RELATION OF THE SPECIMEN.  THE RELATIONSHIP USED IN
       THE PLASTIC REGION IS...     S = B1 + B2*S + B3*S**2
       THIS RELATIONSHIP HAS ALREADY BEEN NORMALIZED SO THAT..B1+B2+B3=1
       THIS ROUTINE CONSISTS OF THREE SEPARATE PARTS.
      COMMON A,A1,A2,A3,A4,A5,AREA1,AREA2,B,B1,B2,B3,B4,B5,BE,C(201,12),
     1C1,C2,CBAR1,CB/R2,CE,CO(11,50),CR,CS,CW,D1,D2,DC,DS,DT,DX,E(201,12
     2),E1,E2,EE(12),EO(11,50),EPS1(200),EPS2(12),ER,ERO(50),ES,ET(12),
     3ETO(50),EW,G,I,II,ID(12),J,K,L,LL,LLL(11),LMAX,LMAX1,LMAX2,M,N,NN,
     4NMAX,NPAGE,NSTORE,P(201,12),P1,P2,PO(11,50),PP,PR,PW,RHO1,PHO2,
     5PHOS,S(201,12),SLOPE,SMAX(201),SO(11,50),SR,SS,SW,SY,T(201,12),T1,
     6T2,TIM(201),TO(11,50),TR,TS,U(201,12),UO(11,50),UR,US,XBAR(11),XO
       FOR A GIVEN IMPACT VELOCITY THIS PART OF THE SUBROUTINE WILL
       COMPUTE THE SPECIMEN STRESS, STRAIN, AND WAVE SPEED.
      IF ((PW/SMAX(L)) .GT. 0.9999999)   GO TO 210
  200 SW=PW
      CW=1.
      EW=E(L,N-1)+SW-S(L,N-1)
      GO TO 290
  210 SW=(((3.*B3*(PW-1.))+(B2+2.*B3)**1.5)**(2./3.)-B2)/(2.*B3)
      CW=1./SQRT(B2+2.*B3*SW)
      EW=B1+B2*SW+B3*SW**2
  290 CONTINUE
      RETURN
       FOR GIVEN CHARACTERISTIC VALUES AT THE BOUNDARIES, THIS PORTION
       OF THE SUBROUTINE WILL COMPUTE THE STRESS AND IMPACT VELOCITY.
      ENTRY PROP
      IF (L-1) 301,301,302
  301 IF ((P2/A4) .GT. 0.9999999)   GO TO 305
  303 P2=P2-P(2,N-1)+S(2,N-1)
      GO TO 300
  302 IF ((P2/A5) .GT. 0.9999999)   GO TO 306
  304 P2=P2-P(LMAX-1,N-1)+S(LMAX-1,N-1)
      GO TO 300
  305 A4=P2
      GO TO 310
  306 A5=P2
      GO TO 310
  300 SP=P2/(P1+1.)
      PP=SP
      GO TO 390
  310 V=P2-1.+(B2+2.*B3)**1.5/(3.*B3)
      X=1.5*B2/B3-(9.*P1**2)/(8.*B3)
      Y=.75*(B2/B3)**2+(9.*P1*V)/(4.*B3)
      Z=.125*(B2/B3)**3-(9.*V*V)/(8.*B3)
      SP=ROOT(X,Y,Z)
  350 PP=1.+((B2+2.*B3*SP)**1.5-(B2+2.*B3)**1.5)/(3.*B3)
  390 CONTINUE
      RETURN
       FOR A GIVEN TIME BASED ON THE SLOPE OF ONE CHARACTERISTIC, THIS
       PORTION OF THE SUBROUTINE WILL COMPUTE THE VALUE OF THE OTHER
       REQUIRED CHARACTERISTIC.
      ENTRY SHIFT
      DT=T(LL,NN)-T(LL,NN-1)
      IF ((S(LL,NN-1)/SMAX(LL)) .GT. 0.9999999)   GO TO 410
  400 IF ((S(LL,NN)/SMAX(LL)) .GT. 0.9999999)   GO TO 402
  401 TR=T(L,N)-DX
      PR=P(LL,NN-1)+(TR-T(LL,NN-1))*(P(LL,NN)-P(LL,NN-1))/DT
```

APPENDIX B

```
      UR=U(LL,NN-1)+(TR-T(LL,NN-1))*(U(LL,NN)-U(LL,NN-1))/DT
      GO TO 480
  402 TR=T(LL,NN-1)+DT*(SMAX(LL)-P(LL,NN-1))/(P(LL,NN)-P(LL,NN-1))
      CSMAX = 1. / SQRT(B2+2.*B3*SMAX(LL))
      PSMAX = 1.+((B2+2.*B3*SMAX(LL))**1.5-(B2+2.*B3)**1.5)/(3.*B3)
      IF (TR+DX-T(L,N))  403,401,401
  403 IF (TR+DX/CSMAX-T(L,N))  406,404,404
  406 X=0.
      Y=(DX/(T(LL,NN)-TR))*(1./C(LL,NN)**3-1./CSMAX**3)
      Z=-1./CSMAX**3+((TR-T(L,N))/(T(LL,NN)-TR))*(1./(C(LL,NN)**3)-
     1 1./CSMAX**3)
      CRI = ROOT(X,Y,Z)
      TR1 = T(L,N) - DX * CRI
      PR = PSMAX + ((TR1 - TR)/(T(LL,NN) - TR)) * (P(LL,NN) - PSMAX)
      TR = TR1
      UR = U(LL,NN-1)+(TR-T(LL,NN-1))*(U(LL,NN)-U(LL,NN-1))/DT
      GO TO 480
  404 PR=PSMAX
      UR=U(LL,NN-1)+(TR-T(LL,NN-1))*(U(LL,NN)-U(LL,NN-1))/DT
      GO TO 480
  410 IF ((S(LL,NN)/SMAX(LL)) .GT. 0.9999999)   GO TO 425
  415 TR = T(L,N) - DX/C(LL,NN-1)
      SR = S(LL,NN-1)
      PR = P(LL,NN-1)
      UR = U(LL,NN-1)
      CR = C(LL,NN-1)
      ER = E(LL,NN-1)
      GO TO 495
  425 X=0.
      Y=(DX/DT)*(1./C(LL,NN)**3-1./C(LL,NN-1)**3)
      Z=-1./C(LL,NN-1)**3+((T(LL,NN-1)-T(L,N))/DT)*(1./(C(LL,NN)**3)  ./
     1(C(LL,NN-1)**3))
      CRI=ROOT(X,Y,Z)
      TR = T(L,N) - DX * CRI
      PR = P(LL,NN-1) + ((TR - T(LL,NN-1))/DT) * (P(LL,NN) - P(LL,NN-1))
      UR=U(LL,NN-1)+(TR-T(LL,NN-1))*(U(LL,NN)-U(LL,NN-1))/DT
  480 IF ((PR/SMAX(LL)) .GT. 0.9999999)   GO TO 490
  485 SR=PR
      CR=1.
      ER=E(LL,NN-1)+SR-S(LL,NN-1)
      GO TO 495
  490 SR=((3.*B3*(PR-1.)+(B2+2.*B3)**1.5)**(2./3.)-B2)/(2.*B3)
      CR=1./SQRT(B2+2.*B3*SR)
      ER=B1+B2*SR+B3*SR**2
  495 CONTINUE
      IF (LL.EQ.1) GO TO 498
      IF (LL.EQ.LMAX) GO TO 499
      RETURN
  498 EE(NN)=EE(NN-1)+(TR-T(LL,NN-1))*(EE(NN)-EE(NN-1))/DT
      RETURN
  499 ET(NN)=ET(NN-1)+(TR-T(LL,NN-1))*(ET(NN)-ET(NN-1))/DT
      RETURN
       END
```

APPENDIX B

```
$IBFTC ROOT     LIST
       FUNCTION ROOT (X,Y,Z)
        FUNCTION ROOT FINDS THE ONE REAL ROOT OF THE CUBIC EQUATION
        X**3 + A*X**2 + B*X + C = 0.  THE ARGUMENT LIST OF THE CALLING
        STATEMENT CONTAINS THE THREE COEFFICIENTS A, B, AND C.
       DOUBLE PRECISION A,B,C,D,E,F
       A=Y/3.-(X/3.)**2
       B=(X/3.)**3-X*Y/6.+Z/2.
       C=B**2+A**3
       IF (C) 10,20,20
    10 PHI=-B/DSQRT(-A**3)
       ROOT=-X/3.+2.*DSQRT(-A)*COS(PHI/3.)
       GO TO 30
    20 D=-B+DSQRT(C)
       E=B+DSQRT(C)
       F=1./3.
       IF (D) 25,22,22
    22 IF (E) 23,24,24
    23 ROOT=-X/3.+D**F+(-E)**F
       GO TO 30
    24 ROOT=-X/3.+D**F-E**F
       GO TO 30
    25 ROOT=-X/3.-(-D)**F-E**F
    30 RETURN
       END
```

APPENDIX C

CALIBRATION OF RECORDING DEVICES

The measurement of stress and particle velocity in each pressure bar is accomplished indirectly by recording transient electrical signals generated by the change in resistance of etched foil strain gages. This technique differs somewhat from the methods employed in the static measurement of strain where the voltage required to "balance" a Wheatstone bridge is proportional to the strain. The transient measurement of strain requires the bridge to be initially balanced and the amount of "unbalance" recorded as the strain is applied.

Each strain-measuring station consists of two strain gages which are connected to opposite arms of a Wheatstone bridge as illustrated schematically in figure C-1(A). Each pair of strain gages is connected to a separate channel of a transducer input conditioner which contains six Wheatstone bridges (B and F Model 1-220B4). The system is calibrated prior to each test by switching known precision resistances into the bridge circuits and recording the resulting deflections on Tektronix Model 531 oscilloscopes equipped with Type D plug-in units. The intensity is modulated every 50 microseconds by means of a separate external oscillator which permits calibration of both the vertical and horizontal axes of the oscilloscope as shown in figure C-1(B).

The equation which describes the output of a bridge with four initially equal arms and two active gages in opposite arms is given by:

$$\frac{\Delta V}{V} = \frac{1}{2} \frac{\Delta R}{R} (1 - n) \qquad (C\text{-}1)$$

where the (1 - n) factor is required to account for the non-linearities which arise for large changes in resistance. This correction factor is given by:

$$(1 - n) = (1 + \frac{\Delta R}{R})^{-1} \qquad (C\text{-}2)$$

The "engineering" strain is proportional to the ratio of the change in resistance to the original resistance of the gage. The constant of proportionality is the gage factor, G, supplied by the manufacturer. Equations (C-1) and (C-2) may be rewritten in terms of strain as:

$$\frac{\Delta V}{V} = \frac{1}{2} G\epsilon \ (1 - n) \qquad (C\text{-}3)$$

and

$$(1 - n) = (1 + G\epsilon)^{-1} \qquad \text{(C-4)}$$

Since the gage factor has a nominal value of two, strains on the order of 2500 microstrain may be measured to within ½ percent when the (1 - n) factor is neglected. Since the strains in the pressure bars never exceeded this value, n was assumed to be equal to zero.

The calibration resistors are wired in parallel with only one of the active arms of the bridge, figure C-1(A). Therefore, the change in resistance of the bridge is only half that which will occur when both gages are strained. The equivalent strain corresponding to a given calibration resistor is given by:

$$\epsilon_{cal} = -\frac{1}{2}\,\frac{R_G}{G(R_G + R_{cal})} \qquad \text{(C-5)}$$

From equation (C-3) we obtain:

$$\left(\frac{\Delta V}{V}\right)_{cal} = \frac{1}{2}\, G\, \epsilon_{cal} \qquad \text{(C-6)}$$

Therefore, the strain is related to the measured change in voltage by eliminating V and G from equations (C-3) and (C-6) to obtain:

$$\epsilon = \frac{\Delta V}{\Delta V_{cal}}\, \epsilon_{cal} \qquad \text{(C-7)}$$

Each strain corresponding to a calibration resistor may be computed from equation (C-5) and the corresponding displacement on an oscilloscope determined experimentally as shown in figure C-1(B).

The elastic wave speed in each pressure bar is determined by impacting each bar separately and observing the multiple reflections of the propagating wave on an oscilloscope sweeping at one millisecond/centimeter. The output of a calibrated external oscillator is superimposed to obtain an accurate time base. An accurate measurement of the length, ℓ, of each pressure bar and the total elapsed time, Δt, between (n + 1) peaks observed in the propagating wave permits the average wave speed to be computed from the expression:

$$c_o = \frac{2\, n\, \ell_o}{\Delta t} \qquad \text{(C-8)}$$

The elastic wave speed for the titanium pressure bars used in these experiments was found by this method to be 2.019×10^5 inches per second.

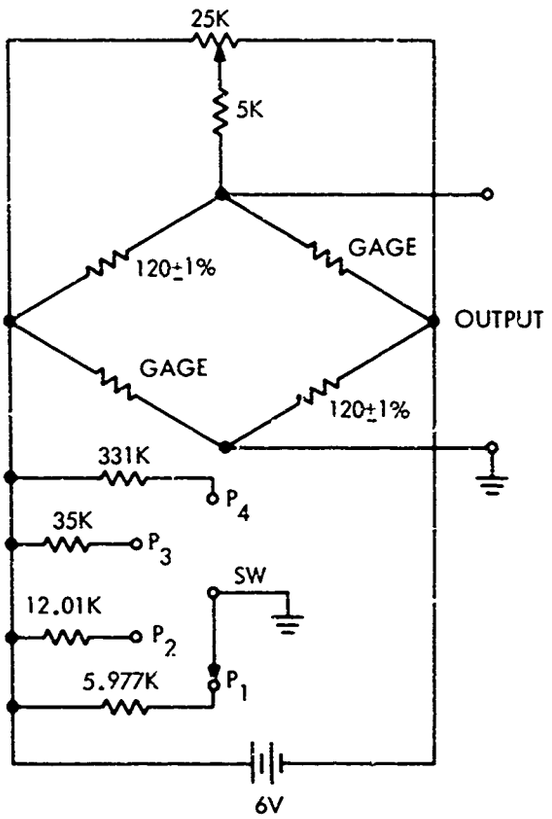

(A) SCHEMATIC DIAGRAM OF TYPICAL CHANNEL OF TRANSDUCER INPUT CONDITIONER

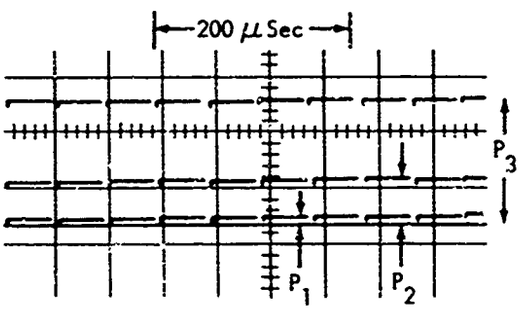

(B) TYPICAL CALIBRATION RECORD ($P_1 = 86.7 \times 10^{-6}$ IN/IN; $P_2 = 817.5 \times 10^{-6}$ IN/IN; $P_3 = 2366.7 \times 10^{-6}$ IN/IN)

FIG.C-1 CALIBRATION OF STRAIN MEASURING EQUIPMENT

APPENDIX D

REFERENCES

1. J. M. Krafft, "Instrumentation for High Speed Strain Measurement," Response of Metals to High Velocity Deformation, Interscience Publishers, New York, 1961, pp. 17-28.

2. F. E. Hauser, J. A. Simmons and J. E. Dorn, "Strain Rate Effects in Plastic Wave Propagation," Response of Metals to High Velocity Deformation, Interscience Publishers, New York, 1961, pp. 93-110.

3. W. J. Gillich, "Plastic Wave Propagation in High Purity Single Crystals of Aluminum " Proceedings of the Fifth U. S. National Congress of Applied Mechanics, The American Society of Mechanical Engineers, New York, 1966, p. 554.

4. J. F. Bell, "An Experimental Diffraction Grating Study of the Quasi-Static Hypothesis of the Split Hopkinson Bar Experiment," Journal of the Mechanics and Physics of Solids, vol. 14, no. 6, Nov 1966, pp. 309-327.

5. T. von Karman, "On the Propagation of Plastic Deformation in Solids," National Defense Research Committee Report No. A-29, 1942.

6. G. I. Taylor, "Propagation of Earth Waves from an Explosion," The Scientific Papers of Sir Geoffrey Ingram Taylor, Cambridge University Press, Cambridge, 1958, pp. 456-463.

7. K. A. Rakhmatulin, "Propagation of a Wave of Unloading," Office of Naval Research, Translation No. 2, Brown University, Providence, Nov 1948.

8. H. Kolsky, "An Investigation of the Mechanical Properties of Materials at Very High Rates of Loading," The Proceedings of the Physical Society, Section B, vol. 62, Part II, no. 359B, 1949, pp. 676-700.

9. A. F. Conn, "On Impact Testing for Dynamic Properties of Metals," Dissertation, The Johns Hopkins University, Baltimore, 1964.

10. J. F. Bell, "On the Direct Measurement of Very Large Strain at High Strain Rates," Experimental Mechanics, vol. 7, no. 1, Jan 1967, pp. 8-14.

11. J. W. Jackson and M. Waxman, "An Analysis of Pressure and Stress Distribution Under Rigid Bridgman-Type Anvils," High Pressure Measurement, Butterworth Inc., 1963, pp. 39-58.

12. J. L. Rand, "An Analysis of the Split Hopkinson Pressure Bar," Dissertation, The University of Maryland, College Park, 1967.

13. R. L. Davis and J. W. Jackson, "A Plastic Stress Analysis of Cylindrical Wafers Under Elastically Deformable Compression Plates," Mechanical Engineering Department Report No. 1965-1, University of Maryland, 1965.

14. M. J. Kenig, "Experiments on Annealed Aluminum," Department of Aerospace and Mechanical Sciences Report Number 737, Princeton University, 1965.

15. J. M. Krafft, A. M. Sullivan and C. F. Tipper, "The Effect of Static and Dynamic Loading and Temperature on the Yield Stress of Iron and Mild Steel in Compression," Proceedings of the Royal Society of London, Series A, vol. 221, 1953, pp. 114-127.

16. U. S. Lindholm, "Some Experiments with the Split Hopkinson Pressure Bar," Journal of the Mechanics and Physics of Solids, vol. 12, 1964, pp. 317-335.

17. K. Tanaka, T. Matsuo, M. Kinoshita and T. Maede, "Strength of Mild Steel at High Strain Rate," Bulletin of the Japan Society of Mechanical Engineers, vol. 9, no. 33, 1966, pp 21-28.

18. R. M. Davies, "A Critical Study of the Hopkinson Pressure Bar," Philosophical Transactions of the Royal Society of London, Series A, vol. 240, 1948, pp. 375-457.

19. G. Fox and C. W. Curtis, "Elastic Strain Produced by Sudden Application of Pressure to One End of a Cylindrical Bar. II. Experimental Observations," The Journal of the Acoustical Society of America, vol. 30, no. 6, Jun 1958, pp. 559-563.

20. W. S. Farren and G. I. Taylor, "The Heat Developed during Plastic Extension of Metals," Proceedings of the Royal Society of London, Series A, vol. CVII, 1925, pp. 422-451.

21. M. J. Kenig and O. W. Dillon, Jr., "Shock Waves Produced by Small Stress Increments in Annealed Aluminum," Journal of Applied Mechanics, vol. 33, Series E, no. 4, Dec 1966, pp. 907-916.

22. C. J. Maiden and S. J. Green, "Compressive Strain Rate Tests on Six Selected Materials at Strain Rates from 10^{-3} to 10^{4} inch/inch/second," Journal of Applied Mechanics, vol. 33, 1966, pp. 496-504.

23. J. F. Bell, "Propagation of Large Amplitude Waves in Annealed Aluminum," Journal of Applied Physics, vol. 31, no. 2, Feb 1960, pp. 277-282.

24. J. F. Bell, "The Dynamic Plasticity of Metals at High Strain Rates: An Experimental Generalization," Behavior of Materials Under Dynamic Loading, The American Society of Mechanical Engineers, New York, 1965, pp. 19-41.

25. S. R. Bodner and R. J. Clifton, "An Experimental Investigation of Elastic-Plastic Pulse Propagation in Aluminum Rods," Transactions of the American Society of Mechanical Engineers, vol. 89, Series E, no. 1, Mar 1967, pp. 91-99.

26. J. F. Bell, "Experimental Study of the Interrelation Between the Theory of Dislocations in Polycrystalline Media and Finite Amplitude Wave Propagation in Solids," Journal of Applied Physics, vol. 32, no. 10, Oct 1961, pp. 1982-1993.

UNCLASSIFIED
Security Classification

DOCUMENT CONTROL DATA - R & D

(Security classification of title, body of abstract and indexing annotation must be entered when the overall report is classified)

1 ORIGINATING ACTIVITY (Corporate author)
U. S. Naval Ordnance Laboratory
White Oak, Silver Spring, Maryland

2a. REPORT SECURITY CLASSIFICATION
UNCLASSIFIED

2b GROUP

3 REPORT TITLE
AN ANALYSIS OF THE SPLIT HOPKINSON PRESSURE BAR

4 DESCRIPTIVE NOTES (Type of report and inclusive dates)

5 AUTHOR(S) (First name, middle initial, last name)
James L. Rand

6 REPORT DATE
2 October 1967

7a. TOTAL NO OF PAGES
78

7b. NO OF REFS
26

8a CONTRACT OR GRANT NO

b. PROJECT NO

c

d.

9a. ORIGINATOR'S REPORT NUMBER(S)
NOLTR 67-156

9b OTHER REPORT NO(S) (Any other numbers that may be assigned this report)

10 DISTRIBUTION STATEMENT
Distribution of this document is unlimited

11 SUPPLEMENTARY NOTES

12 SPONSORING MILITARY ACTIVITY

13 ABSTRACT

The purpose of this paper is to analyze in detail many of the assumptions and techniques often employed to obtain stress-strain relations at rates of strain of approximately 10^3 sec^{-1}. The effects of axial wave propagation and interaction detail in short cylindrical specimens on the resulting stress-strain relation have been evaluated in detail. The effect of specimen geometry on the "end effects" associated with friction has been clearly demonstrated both theoretically and experimentally.

DD FORM 1 NOV 65 1473 (PAGE 1)

S/N 0101-807-6801

UNCLASSIFIED
Security Classification

UNCLASSIFIED
Security Classification

14 KEY WORDS	LINK A		LINK B		LINK C	
	ROLE	WT	ROLE	WT	ROLE	WT
Aluminum						
Dynamic properties						
Split Hopkinson Pressure Bar						
Stress						
Strain						
Friction						
Experimental facilities						
Wave propagation						
Plasticity						
Elasticity						
Method of characteristics						
Constitutive Relations						
Stress-strain relations						

DD FORM 1 NOV 65 1473 (BACK)
(PAGE 2)

UNCLASSIFIED
Security Classification